

**The Potentially Significant Role of CYP3A-Mediated Oxidative Metabolism of
Dabigatran Etexilate and its Intermediate Metabolites in Drug-Drug Interaction
Assessments Using Microdose Dabigatran Etexilate**

Udomsak Udomnilobol, Suree Jianmongkol, Thomayant Prueksaritanont

Department of Pharmacology and Physiology, Faculty of Pharmaceutical Sciences,
Chulalongkorn University, Bangkok, Thailand (U.U., S.J.).

Chulalongkorn University Drug Discovery and Drug Development Research Center
(Chula4DR), Chulalongkorn University, Bangkok, Thailand (U.U., T.P.).

Running title: CYP3A-mediated oxidation of DABE and BIBR0951

Keywords: CYP3A, Dabigatran, Drug-drug interaction, Metabolism, Microdose

Corresponding author: Thomayant Prueksaritanont

Chulalongkorn University Drug Discovery and Drug
Development Research Center (Chula4DR), Chulalongkorn
University, 254 Phayathai Rd., Wangmai, Pathumwan,
Bangkok 10330, Thailand.
Phone: (+66)-02-218-8459
E-mail: thomayant.p@pharm.chula.ac.th

Co-corresponding author: Suree Jianmongkol

Department of Pharmacology and Physiology, Faculty of
Pharmaceutical Sciences, Chulalongkorn University, 254
Phayathai Rd., Wangmai, Pathumwan, Bangkok 10330,
Thailand.
Phone: (+66)-02-218-8318
E-mail: suree.j@pharm.chula.ac.th

Number of text pages: 32

Number of Tables: 3

Number of Figures: 6

Number of Supplemental Tables: 3

Number of Supplemental Figures: 9

Number of References: 24

Number of words in Abstract: 250

Number of words in Introduction: 599

Number of words in Discussion: 1254

Abbreviations: BIBR0951, dabigatran ethylester; BIBR1087, desethyl dabigatran etexilate; BNPP, bis(4-nitrophenyl) phosphate; CES, carboxylesterase; CL_{int} , intrinsic clearance; CTC, clarithromycin; CYP, cytochrome P450; DAB, dabigatran; DABE, dabigatran etexilate; DDI, drug-drug interaction; HIM, human intestinal microsomes; HLM, human liver microsomes; ITZ, itraconazole; KTZ, ketoconazole; PBPK, physiologically-based pharmacokinetics; P-gp, P-glycoprotein; rhCYP, recombinant human cytochrome P450 enzyme

Abstract

Dabigatran etexilate (DABE), a double ester prodrug of dabigatran (DAB), is a probe substrate of intestinal P-glycoprotein (P-gp) commonly used in clinical drug-drug interaction (DDI) studies. When compared to its therapeutic dose at 150 mg, microdose DABE (375 µg) showed approximately 2-fold higher in DDI magnitudes with CYP3A/P-gp inhibitors. In this study, we conducted several *in vitro* metabolism studies to demonstrate that DABE at a theoretical gut concentration after microdosing significantly underwent NADPH-dependent oxidation (~40-50%) in parallel to carboxylesterase-mediated hydrolysis in human intestinal microsomes. Furthermore, NADPH-dependent metabolism of its intermediate monoester BIBR0951 was also observed in both human intestinal and liver microsomes, accounting for 100% and 50% of total metabolism, respectively. Metabolite profiling using LC-MS/MS confirmed the presence of several novel oxidative metabolites of DABE and of BIBR0951 in the NADPH-fortified incubations. CYP3A was identified as the major enzyme catalyzing the oxidation of both compounds. The metabolism of DABE and BIBR0951 was well described by Michaelis-Menten kinetics, with K_m ranging 1-3 µM, significantly below the expected concentrations following the therapeutic dose of DABE. Overall, the present results suggested that CYP3A played a significant role in the presystemic metabolism of DABE and BIBR0951 following microdose DABE administration, thus attributing partly to the apparent overestimation in the DDI magnitude observed with the CYP3A/P-gp inhibitors. Therefore, DABE at the microdose, unlike the therapeutic dose, would likely be a less predictive tool and should be considered as a clinical dual substrate for P-gp and CYP3A when assessing potential P-gp-mediated impacts by dual CYP3A/P-gp inhibitors.

Significant statement

This is the first study demonstrating a potentially significant role of CYP-mediated metabolism of the prodrug DABE following a microdose, but not a therapeutic dose. This additional pathway coupled with its susceptibility to P-gp may make DABE a clinical dual substrate for both P-gp and CYP3A at a microdose. The study also highlights the need for better characterization of the pharmacokinetics and metabolism of a clinical DDI probe substrate over the intended study dose range for proper result interpretations.

Introduction

Dabigatran etexilate (DABE) is an orally bioavailable direct thrombin inhibitor used at 75-300 mg for treatments of deep vein thrombosis and pulmonary edema. It is designed as a double ester prodrug because of a poor oral bioavailability of its active moiety, dabigatran (DAB) (FDA, 2010a). After absorption, DABE has been shown to undergo two sequential hydrolysis by carboxylesterase (CES) enzymes to liberate DAB into the systemic circulation (Figure 1) (Laizure et al., 2014). DABE is known to be primarily hydrolyzed by the intestinal CES2 enzyme to form an intermediate monoester metabolite called dabigatran ethylester (BIBR0951), which is further converted to DAB by the hepatic CES1 enzyme. To a much lesser extent, DAB can also be formed through the hydrolysis of another intermediate monoester metabolite, desethyl dabigatran etexilate (BIBR1087). The prodrug DABE, but not the active drug DAB, was shown *in vitro* and through several clinical drug-drug interaction (DDI) studies following the therapeutic dose (150-300 mg) of DABE to be a substrate of the human intestinal efflux transporter P-glycoprotein (P-gp) (Hartter et al., 2013; Ishiguro et al., 2014; Hodin et al., 2018). Citing its sensitivity and selectivity to intestinal P-gp, worldwide regulatory agencies have recommended DABE as a clinical probe substrate for investigating the perpetrator's potential on intestinal P-gp inhibition (EMA, 2012; FDA, 2020a).

Recently, a microdose DABE (375-750 μ g) has been utilized for studying DDI as well as phenotyping intestinal P-gp function in several populations (Prueksaritanont et al., 2017; Rattanacheworn et al., 2021; Tatosian et al., 2021). Interestingly, the systemic exposure following a microdose DABE was approximately 2-fold lower than expected from its therapeutic dose, suggesting a non-linear PK (Prueksaritanont et al., 2017). Furthermore, DDI magnitudes after the microdose DABE and P-gp inhibitors, i.e., clarithromycin (CTC) and itraconazole (ITZ), were higher than those observed using the therapeutic dose. In the microdose study, CTC increased the area under the plasma concentration-time curve of DAB

by 4 fold (Prueksaritanont et al., 2017), as compared to <2 fold under the therapeutic dose condition (FDA, 2010a; Delavenne et al., 2013). Two hypotheses have been proposed for the dissimilar interaction magnitudes following two different doses of DABE (Prueksaritanont et al., 2017). First, the intestinal P-gp is partially saturated at high doses of DABE, but fully active when the intestinal concentration of DABE is relatively low following the microdose. The DDI magnitudes are thus increased through the maximal inhibition of intestinal P-gp following microdose DABE administration (Prueksaritanont et al., 2017). A recent published literature using physiologically-based pharmacokinetic (PBPK) modeling suggested that regional differences in P-gp inhibition could possibly explain the different magnitudes of DABE-CTC interaction between microdose and standard dose of DABE (Lang et al., 2021). However, Prueksaritanont et al. hypothesized that CYP3A could be involved and contribute to the nonlinearity and the disparity in DDI magnitudes in the presence of either CTC or ITZ after the microdose DABE administration (Prueksaritanont et al., 2017), based on the following two reasons: 1) apart from being P-gp inhibitors, CTC and ITZ are also potent inhibitors of CYP3A enzymes (Ke et al., 2014), and 2) using a recombinant enzyme system, CYP3A4-mediated DABE oxidation was reported, albeit as an insignificant metabolic pathway when studied at a relatively high concentration (Blech et al., 2008; FDA, 2010a). Nevertheless, this hypothesis has not been thoroughly investigated elsewhere.

In this study, the oxidative metabolism of DABE and its intermediate metabolites (BIBR0951 and BIBR1087) was investigated using an *in vitro* approach to explore whether CYP3A-mediated metabolism is a potential underlying mechanism for the disparity in DDI magnitudes of DABE-P-gp inhibitor (CTC and ITZ) following administration of the microdose and the therapeutic dose of DABE.

Materials and Methods

Materials

All materials used in this study were the highest grade available commercially. Dabigatran etexilate (DABE), desethyl dabigatran etexilate (BIBR1087), dabigatran ethylester (BIBR0951), and dabigatran (DAB) were purchased from Toronto Research Chemical Inc. (Ontario, Canada). Acetonitrile was purchased from Honeywell Burdick and Jackson (Fischer Scientific, MI, USA). β -Nicotinamide adenine dinucleotide phosphate tetrasodium salt (NADPH), ketoconazole (KTZ), labetalol hydrochloride, and formic acid were purchased from Tokyo Chemical Industry Co., Ltd. (Chuo-ku, Tokyo, Japan). Bis(4-nitrophenyl) phosphate (BNPP) was purchased from Sigma Aldrich (St. Louis, MO, USA). Pooled human liver microsomes (HLM) were purchased from Gibco Life Technologies (Thermo Fischer Scientific Inc., MA, USA). Recombinant human CYP3A4 and CYP3A5 with oxidoreductase and cytochrome b_5 (Corning[®] Supersome[™]) and pooled human intestinal microsome (HIM) were purchased from Corning Incorporated (NY, USA).

In vitro metabolic stability

The metabolism of DABE and its monoester metabolites (BIBR1087 and BIBR0951) was investigated in human liver microsomes (HLM), human intestinal microsome (HIM), and recombinant human CYP3A4 (rhCYP3A4) and CYP3A5 (rhCYP3A5) enzymes. Briefly, the 100- μ L reaction mixtures were prepared to obtain a final concentration of 0.1 M potassium phosphate buffer (pH 7.4), 3.3 mM $MgCl_2$, and specific protein concentration in the presence or absence of 1.3 mM NADPH. The HLM concentration was at 0.025, 0.2, and 0.5 mg/mL for DABE, BIBR0951, and BIBR1087, respectively. For HIM incubation, the protein concentration was at 0.05 mg/mL for DABE, and at 0.1 mg/mL for both BIBR0951 and BIBR1087. The final rhCYP3A4 concentration was 5 pmol/mL for both DABE and

BIBR0951, whereas the rhCYP3A5 concentration was at 20 and 5 pmol/mL for DABE and BIBR0951, respectively. After pre-warming at 37°C for 10 min, the reactions were initiated by addition of compound. The organic solvent (acetonitrile) in the reactions was kept constant at 1%. After incubation, the reactions were quenched with one volume of ice-cold acetonitrile + 0.1 % formic acid containing labetalol as an internal standard. Then, the supernatants of reaction mixtures were collected by centrifugation, and diluted with an appropriate volume of water + 0.1% formic acid prior to LC-MS/MS analysis. The natural logarithm of peak area ratios of the analytes to the internal standard were plotted against incubation time points. The first-order depletion rate constant (k_{dep}) was estimated from the slope of the graph using linear regression analysis. The *in vitro* intrinsic clearance (CL_{int}) of the compounds was calculated from the formula: $k_{\text{dep}} \times (\text{incubation volume})/(\text{mg of microsomal protein or pmol of recombinant enzyme})$.

In some experiments, the reactions were co-incubated either with 100 μM BNPP (non-specific CES inhibitor) or 1 μM KTZ (selective CYP3A inhibitor) to investigate the involvement of CES and CYP3A enzymes to overall microsomal metabolism.

***In vitro* enzyme kinetic studies**

Kinetic parameters of CES-mediated hydrolysis of DABE and BIBR0951 were determined in HIM and HLM incubations without NADPH under the linear conditions for metabolite formation. The experiments were conducted as described under the section of *in vitro* metabolic stability, by varying substrate concentrations from 1-400 μM . The Michaelis-Menten constants (K_m) and maximum velocity (V_{max}) were estimated from a graph plotted between rates of metabolite formation versus the corresponding substrate concentrations, using a 2-parameter hyperbolic equation in the SigmaPlot software version 13.0 (SyStat Software, Inc., CA, USA).

Kinetic parameters of CYP3A-mediated oxidative metabolism of DABE and BIBR0951 were determined in the NADPH-fortified rhCYP3A4/5 incubations by a substrate depletion method, as described previously (Obach and Reed-Hagen, 2002). Briefly, the experiments were performed using the procedure described under the section of *in vitro* metabolic stability, except that the substrate concentrations were varied from 0.1-30 μ M. The first-order depletion rate constants (k_{dep}) were plotted against the corresponding substrate concentrations. The K_m was estimated from the inflection points of non-linear curve fitting from a 4-parameter Hill equation using the SigmaPlot software. The V_{max} was calculated from multiplying K_m to the CL_{int} value obtained from the incubation at the lowest substrate concentration tested (0.1 μ M).

Quantitative LC-MS/MS bioanalysis

DABE and its metabolites in the samples were quantified by AB SCIEX QTRAP6500+ LC-MS/MS system. The chromatographic separation was performed by Exion LC AD100 system coupled with Phenomenex Kinetex[®] C-18, 1.3 μ m, 50 \times 2.1 mm analytical column. For mobile phases, the flow rate was set at 0.3 mL/min using a binary system of water and acetonitrile (both were fortified with 0.1% formic acid) as phase A and B, respectively. The gradient program was set as equilibration at 5% B for 0.5 min, linear gradient 5-50% B for 3.5 min, ramping to 95% B for 1 min, holding at 95% B for 1 min, column reconditioning to 5% B for 0.2 min, and post-analysis equilibration at 5% B for 0.8 min. The Turbo VTM ion source was operated in the electrospray positive ionization mode under 40 psi of curtain gas, 4500 volts of ion spray voltage, 450°C of source temperature, and 40 psi for both heating and nebulizing gases. The peak area of analytes was acquired by a multiple reaction monitoring (MRM) mode, using ion transitions and compound-specific MS parameters (i.e., declustering potential, entrance potential, collision energy, and collision exit

potential) obtained from automatic compound optimization following direct infusion of analytical standards. For commercially unavailable metabolites, the quantification was relative based on MRM transitions of their parents. Data were processed by Analyst version 1.6 and MultiQuant version 3.0 softwares (AB SCIEX, MA, USA).

Metabolite identification

Oxidative metabolites in the samples at the longest incubation time were identified using AB SCIEX X500B QTOF LC-MS/MS system. The chromatographic separation was performed by Exion LC AD100 system coupled with Phenomenex Kinetex[®] C-18, 1.7 μ m, 50 \times 2.1 mm analytical column. For mobile phases, the flow rate was set at 0.4 mL/min using a binary system of water and acetonitrile (both were fortified with 0.1% formic acid) as phase A and B, respectively. The gradient program was similar as described under the section of quantitative LC-MS/MS bioanalysis. The Turbo VTM ion source was operated in the electrospray positive ionization mode under 40 psi of curtain gas, 4500 volts of ion spray voltage, 7 psi of collision gas, 450°C in temperature, and 40 psi for both heating and nebulizing gases. An information-dependent data acquisition (IDA) method was applied for metabolite identification. A full scan TOF MS ranging from m/z 50-1,000 was used as a survey scan using declustering potential and declustering potential spread of 60 and 20 V, respectively. The product ion spectra were acquired for the m/z ranged 50-1,000 using collision energy and collision energy spread at 35 and 15 V, respectively. The data were processed and interpreted using SCIEX OS version 1.6 and MetabolitePilotTM version 2.0 softwares (AB SCIEX, MA, USA).

Statistical analysis

Data were expressed as mean \pm standard deviation (SD) from at least three independent experiments ($n \geq 3$). The statistical analysis was performed by IBM SPSS® Statistics 22 (Armonk, NY, USA) using the independent *t*-test or one-way analysis of variance (ANOVA) followed by a post-hoc Bonferroni test, where appropriate. Statistical significance was considered at *p*-value < 0.05 .

Results

NADPH-dependent metabolism of DABE and its intermediate metabolites in HIM and HLM

To investigate an involvement of NADPH-dependent metabolic pathways in metabolism of DABE and its intermediate metabolites (BIBR1087 and BIBR0951), the metabolic stability assay was first conducted by separately incubating each compound at 1 μ M, a concentration falling within the intestinal concentration range estimated following the microdose (see Discussion), with HIM and HLM in the presence or absence of NADPH. For all three compounds, enzyme-mediated reactions were confirmed based on minimal parent disappearance and no detectable metabolite formation observed in the incubations without microsomal protein (Supp. Figure 1).

DABE metabolism

In HIM incubations, DABE disappearance was faster in the presence of NADPH than in the absence of NADPH, with the CL_{int} value differing by ~ 1.6 -fold (Figure 2A and Table 1). However, the formation of its major metabolite, BIBR0951, was comparable under these two conditions. Another intermediate metabolite BIBR1087 was also observed, albeit at a much lower extent ($<3\%$ of DABE) (Figure 2A). The results suggested that in HIM, DABE underwent both NADPH-independent, primarily to BIBR0951 and to a much lesser extent to BIBR1087, as well as NADPH-dependent metabolism, to others yet to be identified metabolites. In HIM, the relative contribution of NADPH-dependent metabolic pathways constituted $\sim 40\%$ of the overall DABE metabolism (Table 1).

In HLM incubations, DABE was comparably metabolized in the presence and absence of NADPH to form BIBR1087 as a major metabolite, while BIBR0951 and DAB were barely detected (Figure 2A). There was no significant difference between the 2

incubation conditions in either DAB disappearance or formation of its metabolites BIBR0951 and BIBR1087 (Figure 2A and Table 1), suggesting that unlike HIM, the metabolism of DAB in HLM was mediated primarily by non-NADPH dependent enzymes and mainly to BIBR1087.

BIBR0951 metabolism

In HIM incubations, BIBR0951 disappearance was pronounced (~40% consumption in 10 min) in the incubation fortified with NADPH, but very minimal in the absence of NADPH (Figure 2B and Table 1). DAB formation in both incubations with and without NADPH was very low (Figure 2B). In HLM incubations with BIBR0951, there was a more rapid consumption of BIBR0951, resulting in 2-fold higher in the CL_{int} in the presence than in the absence of NADPH (Figure 2B and Table 1). However, its hydrolytic metabolite (DAB) was formed at a similar level in the HLM incubations with and without NADPH (Figure 2B). These results suggested that in both HIM and HLM incubations, in addition to CES-mediated hydrolysis, NADPH-dependent enzymes were likely involved in the metabolism of BIBR0951 to some unidentified metabolites. Additionally, the formation of DAB in both HIM and HLM was mediated primarily by hydrolytic enzymes.

BIBR1087 metabolism

In HIM incubations, the disappearance of BIBR1087 was 68% higher with NADPH than that without NADPH, whereas DAB formation was comparable between the two incubation conditions (Figure 2C and Table 1). Unlike HIM incubations, there was no difference in both BIBR1087 disappearance and DAB formation (Figure 2C and Table 1) in the HLM incubations with and without NADPH. These results indicated that BIBR1087 underwent metabolism by NADPH-dependent enzymes only in the HIM, but not in the HLM.

DAB, the major metabolite of BIBR1087, was likely generated via hydrolytic enzymes in both the HIM and the HLM.

Identification of oxidative metabolites of DABE and BIBR0951 in HIM and HLM

Oxidative metabolites in the incubation with BIBR0951

We first identified the NADPH-dependent metabolites of BIBR0951 generated in HIM which included M324, M488, M400, M516 (1), M416, M516 (2), M498 (1), M498 (2), and M514 (Figure 3A). The key product ions of BIBR0951 and its metabolites are listed in Supp. Table 1. A fragmentation pattern of the BIBR0951 showed the intense daughter ions of its core structure at the m/z 289.10 and 306.11 amu, and a weak ion of ethyl 3-(pyridin-2-ylamino)propanoate ion at the m/z 195.11 amu. All oxidative metabolites found also showed the product ion at the m/z 289.10, suggesting that the core structure was intact and the oxidation occurred on the surrounding functional groups. The most abundant oxidative metabolite, M400, was an *N*-dealkylated metabolite with a loss of 100 amu, equivalent to *N*-(ethyl propionate) group ($C_5H_8O_2$). The M516 (1) and M516 (2) shared the common mass shift of +16 amu or hydroxylation. For M516 (1), the presence of product ions at the m/z 289.10 and 306.13 amu suggested that the hydroxylation could occur on either *N*-(ethyl propionate) or pyridine moiety. In the case of M516 (2), its product ion at the m/z 193.0978 amu indicated the hydroxylation on an aliphatic carbon of the *N*-(ethyl propionate) moiety, which possibly dehydrated during MS fragmentation. Both M498 (1) and M498 (2) showed a mass shift of -2 amu, which could result from dehydrogenation, or oxidation followed by dehydration. The presence of product ions at the m/z 289.10 and 306.13 amu pointed to the metabolic site on the *N*-(ethyl propionate) moiety. For other oxidative metabolites (M324, M488, M416, and M514), the product ions indicated that they were the secondary metabolites of BIBR0951. A mass shift of -176 amu of M324 corresponded to a dual loss of pyridine and

N-(ethyl propionate) moieties, while M488 and M416 were the hydroxylated versions (+16 amu) of DAB and M400, respectively. For M514, a mass shift of +14 indicated an addition of 1 atomic oxygen plus a loss of 2 hydrogen atoms, possibly generated from either M516 or M498.

In the HLM incubation, all primary oxidative metabolites of BIBR0951 (including M400, M516 (1), M516 (2), M498 (1), and M498 (2)) were detected only in the presence of NADPH (Figure 3B). The M400 was still the most abundant oxidative metabolite detected in the HLM incubation. In addition, none of the secondary oxidative metabolites of BIBR0951 (M324, M488, and M416) was observed in the HLM incubation, except the M514 (Figure 3B).

Oxidative metabolites in the incubation with DABE

In HIM, there were 5 oxidative metabolites, including M400, M644 (1), M644 (2), M264, and M528, with M400 and M264 being major products (Figure 4A). After MS/MS fragmentation, the parent DABE showed 3 dominated daughter ions at the m/z 289.11, 434.22, and 526.22 amu (Supp. Table 2). Based on both MS/MS spectra and retention time, M400 was the same oxidative metabolite found in the microsomal incubation with BIBR0951, suggesting that M400 was a secondary metabolite of DABE generated subsequently from BIBR0951. Although a small peak of M264 was also detected in all HIM incubations with DABE, an increase of its peak intensity over time in the incubation with NADPH supported that M264 was an oxidative metabolite of DABE. The molecular ion at the m/z 264.1707 amu corresponded to a structure of hexyl ((4-aminophenyl)(imino)methyl)carbamate, possibly formed by an oxidative *N*-dealkylation on the aliphatic carbon adjacent to the 1-methyl-1H-benzo[d]imidazole ring (Supp. Table 2). The M644 (1) and M644 (2) shared a common mass shift of +16 amu or addition of an

atomic oxygen (hydroxylation). The common product ion at the m/z 526.22 suggested that hydroxylation could be assigned on two different aliphatic carbons of the hexyl carbamate moiety (Supp. Table 2). For M528, a neutral loss of 100 amu from both mother and daughter m/z indicated a cleavage of *N*-(ethyl propionate) group ($C_5H_8O_2$) through an oxidative *N*-dealkylation reaction (Supp. Table 2).

In HLM, all oxidative metabolites found were detected in the HIM, with M264 showing the highest intensity (Figure 4B).

Investigation of CYP3A-mediated oxidative metabolism of DABE and BIBR0951 using chemical inhibitors.

Effects of chemical inhibitors on DABE metabolism

Given the oxidative metabolism of DABE occurred primarily in the HIM, we next investigated the potential involvement of CYP3A in the HIM metabolism of DABE. In the presence of KTZ, a known CYP3A inhibitor, DABE disappearance in the HIM incubation with NADPH was inhibited by 53% when compared to the solvent control (Figure 5A and Table 1). KTZ drastically inhibited the formation of BIBR1087 but exerted a little effect on BIBR0951 formation (Supp. Figure 2A&D). In addition, KTZ completely inhibited the formation of all primary oxidative metabolites of DABE (Supp. Figure 2B, C, and E). As expected, BNPP, a known CES inhibitor, had no effect on the formation of the primary oxidative metabolites of DABE (i.e. M644 (1), M644 (2), M264, and M528) (Supp. Figure 2B, C, and E). These results suggested that CYP3A was the predominant NADPH-dependent enzyme responsible for the oxidative metabolism of DABE to form BIBR1087 and other oxidative metabolites (M644 (1), M644 (2), M264, and M528).

Effects of chemical inhibitors on BIBR0951 metabolism

In the NADPH-fortified HIM incubation, KTZ inhibited BIBR0951 metabolism by 88% (Figure 5B and Table 1), and completely abolished the formation of all primary oxidative metabolites of BIBR0951 (i.e. M400, M516 (1), M516 (2), M498 (1), and M498 (2)) (Supp. Figure 3B-F) but with minimal effect on the formation of DAB (Supp. Figure 3A). In contrast, BNPP had modest effects on both BIBR0951 disappearance (Figure 5B and Table 1) and DAB formation (Supp. Figure 3A). Interestingly, both KTZ and BNPP were able to inhibit the formation of DAB in the incubation without NADPH (Supp. Figure 3A).

In NADPH-fortified HLM incubation, KTZ significantly decreased BIBR0951 disappearance by ~58% but had no effect on DAB formation (Figure 5C, Table 1, and Supp. Figure 4A). In addition, KTZ completely inhibited the formation of the primary oxidative metabolites of BIBR0951 (Supp. Figure 4B-F). In this system, BNPP significantly reduced BIBR0951 disappearance by 40% and dramatically decreased DAB formation (Figure 5C, Table 1, and Supp. Figure 4A). As expected, BNPP had no effect on the formation of the primary oxidative metabolites of BIBR0951 (Supp. Figure 4B-F). In HLM incubation without NADPH, BNPP significantly inhibited CES-mediated BIBR0951 hydrolysis by decreasing both BIBR0951 disappearance and DAB formation by more than 80%. Under the same incubation condition, KTZ had minimal effects on both BIBR0951 disappearance and DAB formation (Figure 5C, Table 1, and Supp. Figure 4A). Notably, the CL_{int} of BIBR0951 calculated from the HLM incubation without NADPH was comparable to that obtained from the HLM incubation with NADPH and KTZ (Table 1).

Therefore, these results indicated that the oxidative metabolism of BIBR0951 observed earlier in HIM and HLM incubations was mediated through CYP3A enzymes. In addition, CYP3A also partly metabolized BIBR0951 to DAB.

Investigation of CYP3A-mediated oxidative metabolism of DABE and BIBR0951 using recombinant enzymes.

To further confirm CYP3A-mediated DABE and BIBR0951 oxidation, DABE and BIBR0951 at 1 μ M were incubated with recombinant human CYP3A4 (rhCYP3A4) and CYP3A5 (rhCYP3A5) enzymes.

NADPH-dependent disappearance of DABE and BIBR0951 was clearly observed in both rhCYP3A4 and rhCYP3A5 incubations (data not shown), confirming the roles of both CYP3A isoforms in the oxidative metabolism of DABE and BIBR0951. When the intersystem extrapolation factor (ISEF) and enzyme abundance were considered for comparison the relevance of two isoforms (Bohnert et al., 2016), DABE and BIBR0951 were oxidative metabolized mainly by CYP3A4 but with a lesser extent by CYP3A5.

As shown in Figure 4C-D, all primary oxidative metabolites of DABE (including M644 (1), M644 (2), M264, and M528) were detected in both rhCYP3A4 and rhCYP3A5 systems, with M264 and BIBR1087 being the major metabolites. Interestingly, the peaks of BIBR0951 and BIBR1087 in the NADPH-fortified rhCYP3A4/5 incubations were higher than those in the NADPH-free incubations, suggesting that BIBR0951 and BIBR1087 were formed, at least partly, by CYP3A4/5-mediated ester cleavage of DABE.

As shown in Figure 3C-D, both rhCYP3A4 and rhCYP3A5 could catalyze the formation of all primary oxidative metabolites of BIBR0951 detected in HIM and HLM, with M400 being the most abundant metabolite. Interestingly, the metabolite M516 (1) and M498 (2) were formed by only rhCYP3A4, but not rhCYP3A5. Furthermore, the intensity of DAB in NADPH-fortified rhCYP3A4/5 incubations was higher than that in NADPH-free incubations, indicating that DAB was formed minorly through CYP3A4/5-mediated ester cleavage of BIBR0951.

Determination of kinetic parameters of CES- and CYP3A4/5-mediated metabolism of DABE and BIBR0951

We next determined the enzyme kinetic parameters, especially the Michaelis-Menten constants (K_m) of CYP3A4/5-mediated oxidation (determined based on substrate depletion as well as metabolite formation) and compared them to those of CES-mediated hydrolysis of DABE and BIBR0951 (determined based on metabolite formation).

For DABE, the K_m values for rhCYP3A4- and rhCYP3A5-mediated DABE depletion as determined were 1.4 and 1.1 μM respectively (Table 2 and Supp. Figure 5A), comparable to or lower than the K_m values for both intestinal and hepatic CES-mediated DABE hydrolysis (1-3 and 8-9 μM for BIBR0951 and BIBR1087 formation, respectively) (Table 2 and Supp. Figure 6A-B). Of note, the K_m value for DABE hydrolysis in HIM of this study (1.2 μM) was about 7 fold lower than reported previously (8.6 μM) (Laizure et al., 2014), possibly due to the batch-to-batch variation in HIM quality and preparation (Hatley et al., 2017).

For BIBR0951, the K_m values for rhCYP3A4- and rhCYP3A5-mediated BIBR0951 depletion were at 2.8 and 0.6 μM (Table 2 and Supp. Figure 5B), respectively. The values were 185- and 863-fold lower than that for CES-mediated DAB formation in HLM (Table 2 and Supp. Figure 6C). The K_m for CES-mediated DAB formation in HIM was not determined given the very low formation of DAB in this system.

In the rhCYP3A4/5 systems, the K_m values based on metabolite formation following incubation with DABE and BIBR0951 ($<5 \mu\text{M}$, Supp. Table 3 and Supp. Figure 7-8) were in line with those observed based on substrate depletion. Overall, the findings suggested that CYP3A4/5-mediated metabolism in HIM and HLM could play an important role at relatively low concentrations of DABE and BIBR0951, while CES-mediated hydrolysis could become dominant at higher concentrations of both compounds.

Investigation of saturation of CYP3A4/5-mediated oxidative metabolism of DABE and BIBR0951

We next quantified the relative contribution of CYP3A to overall microsomal metabolism at various concentrations of DABE and BIBR0951 (1, 10, and 100 μ M). As illustrated in Table 3, DABE at the concentration of 1 μ M was metabolized in HIM by both CES and CYP3A with the relative contribution of CYP3A at 38%. By increasing the concentration of DABE from 1 to 10 μ M, the involvement of CYP3A was decreased from 38% to 19%. Due to a solubility limit of DABE, the CL_{int} of DABE disappearance and the relative contribution of CYP3A were not evaluated at the concentration of 100 μ M.

In HIM incubations, BIBR0951 was entirely metabolized by CYP3A (100% contribution) at all concentrations tested (1, 10, and 100 μ M) (Table 3). In HLM, the relative contribution of CYP3A was about 52% when BIBR0951 was incubated at the concentration of 1 μ M, but significantly reduced to 15% at the concentration of 10 μ M. At the high concentration of BIBR0951 (100 μ M), CYP3A-mediated BIBR0951 oxidation was completely abolished, and BIBR0951 was solely metabolized by NADPH-independent hydrolysis (Table 3).

These results supported that at relatively low substrate concentrations, both CES and CYP3A enzymes contributed significantly to the metabolism of DABE (in HIM) and BIBR0951 (in HLM). However, when the concentrations were increased beyond 10 μ M, the CYP3A-mediated oxidation was saturated, and the metabolism of DABE and BIBR0951 in HIM and of DABE in HLM was mediated almost exclusively by CES enzymes.

Discussion

In this study, we utilized several *in vitro* techniques to demonstrate that DABE and its intermediate metabolites (primarily BIBR0951, the major gut metabolite) underwent substantial CYP3A-mediated metabolism in HIM. Additionally, a significant extent of BIBR0951 oxidation was also observed in HLM. The oxidative metabolism was saturable at a concentration range similar to the estimated intestinal concentrations following microdosing at 375 ug, supporting the earlier postulation that CYP3A might be involved in and contribute to the nonlinearity of DAB PK and the greater increase of DAB exposure by CTC and ITZ with the microdose *versus* with the therapeutic dose of DABE (Prueksaritanont et al., 2017).

Shown in Figure 6 is a comprehensive metabolic scheme proposed based on the present *in vitro* findings. Overall, DABE is metabolized in the intestine by both CYP3A4/5 and hydrolysis (presumably the CES2-mediated pathway) with CYP3A4/5 accounting for approximately 40-50% of the overall gut metabolism. The CYP3A4/5 enzymes catalyze the formation of several oxidative metabolites of DABE (M644 (1), M644 (2), M264, and M528); these findings have never been reported previously either *in vitro* (FDA, 2010b; Hu et al., 2013) or *in vivo* (Blech et al., 2008; FDA, 2010a; FDA, 2010b). As demonstrated previously (Laizure et al., 2014), the hydrolysis of DABE by intestinal CES2 enzymes yields BIBR0951, which was subsequently metabolized exclusively by CYP3A4/5 in the small intestine to form several novel oxidative metabolites (M400, M516 (1), M516 (2), M498 (1), and M498 (2)), along with DAB. The formation of another intermediate monoester BIBR1087 from DABE in the gut is minimal, and the reaction was mediated by both CES and CYP3A enzymes. In the liver, DABE is hydrolyzed mainly by the CES1 enzyme to form BIBR1087, which further liberates the active DAB via CES2-mediated hydrolysis (Laizure et al., 2014). CYP3A4/5 involvement in BIBR1087 metabolism in the liver is very limited. Unlike DABE, BIBR0951 is metabolized in the liver to a similar extent by both CES1 and

CYP3A4/5 enzymes. The DAB formation pathway through BIBR0951 by CES1 is more pronounced than that via CYP3A4/5 enzymes. In addition, the metabolism of BIBR0951 by hepatic CYP3A4/5 yields the same oxidative products as those formed in the gut epithelia. Notably, the CYP3A4/5-mediated oxidative metabolism of both DABE and BIBR0951 in the small intestine and of BIBR0951 in the liver, was shown to be saturable especially when the concentrations of both compounds exceeding 10 μ M (exceeding the K_m values of CYP3A4/5).

Among the oxidative metabolites identified in this study, the M400 (*N*-dealkylated metabolite of BIBR0951) was the most abundant metabolite. Noteworthy that the previous literature proposed that M400 was formed by direct DAB oxidation *in vivo* (Blech et al., 2008). However, our *in vitro* results demonstrated that DAB was metabolically stable in HLM (Supp. Figure 9), with no metabolite detected. In addition, DAB was also reportedly not being metabolized by any CYP isoform (FDA, 2010a). A human ADME study following IV administration of DAB also confirmed that DAB is excreted mainly unchanged (>90% of dose) with less than 4% recovered as oxidative (but not M400) metabolites (Blech et al., 2008). Therefore, M400 is likely originated from CYP3A4/5-mediated BIBR0951 oxidation, rather than from the direct oxidation of DAB. Noteworthy that M400 was also found following oral administration of radiolabeled DABE at 200 mg, with recoveries of 0.2% and 5.8% of dose in the urine and feces, respectively (Blech et al., 2008). Although the *in vivo* formation of M400 has never been reported under the microdose condition, we expect that it could be formed more significantly when compared to the therapeutic dose condition.

The *in vitro* metabolism data obtained in this study (Figure 6) may shed some light on the disparity in the DDI magnitude by CTC and ITZ following microdose vs following the therapeutic dose of DABE. After oral administration of microdose DABE at 375 μ g, the theoretical gut concentration of DABE and BIBR0951 is approximately at 2.4 μ M (FDA,

2020b), or even lower when considering an intestinal P-gp mediated DAB efflux. Under this condition, the pathways of CYP3A4/5-mediated DAB and BIBR0951 oxidation may compete with the typical DAB formation pathway, possibly resulting in the lower systemic exposure of DAB following microdose DAB than expected from the therapeutic dose DAB. In the presence of either CTC or ITZ, the DDI magnitude following microdose DAB would be magnified from their inhibitory effects on CYP3A4/5-mediated oxidative metabolism of DAB and BIBR0951, in addition to P-gp. On the contrary, following oral administration of a therapeutic dose DAB at 150 mg (the expected gut concentrations >100 μ M), the relative contribution of CYP3A4/5 to overall disposition is expected to be insignificant, and therefore the P-gp-mediated DAB efflux is the major mechanism producing the DDI magnitude.

Using a semi-mechanistic PBPK model, a previous study proposed that the higher magnitudes of microdose DAB-CTC DDI could arise from the regional difference in P-gp inhibition (Lang et al., 2021). In the present study, a comprehensive *in vitro* data set supported another possibility that the disposition of microdose DAB may not rely solely on the intestinal P-gp-mediated DAB efflux, but also depends on the CYP3A-mediated oxidative metabolism of DAB and its intermediate BIBR0951. Furthermore, an interplay between CYP3A4/5 and P-gp in the gut may possibly occur for DAB, and thus increasing the complexity of its disposition following the microdose administration. However, the relative significance of each pathway (P-gp and CYP3A4/5) to the overall disposition of microdose DAB remains to be investigated, via either a clinical study or PBPK modeling or both.

Although the microdosing approach provides some advantages in early drug development in terms of safe assessment in first-in-human PK and DDI evaluations, there are several previous cases showing that their PK following microdose were not in line with those

following therapeutic dose (Burt et al., 2020). According to the previous meta-analysis of 46 drugs administered orally, the microdose PK of 13 drugs (32%) could not be linearly extrapolated from the PK at therapeutic dose, mostly caused by saturation of enzymes and/or transporters at the therapeutic dose (van Nuland et al., 2019). In addition to those known cases, our *in vitro* findings for DABE and its metabolites exemplified another case that the saturation of CYP3A and/or P-gp could be the underlying mechanisms of nonlinearity and a disparity in DDI magnitude following microdose vs following therapeutic dose. It is worth pointing out that dual P-gp and CYP3A inhibitors, like dual P-gp and CYP3A substrates, are commonly found (Yasuda et al., 2002; Vermeer et al., 2016), and thus the microdose DABE remains a valuable clinical tool for DDI assessments, although with different interpretations from when using the therapeutic dose DABE. No substantial differences in result interpretations are anticipated when using either the microdose or therapeutic doses of DABE with selective P-gp inhibitors.

In conclusion, DABE and its gut intermediate monoester BIBR0951 were significantly metabolized by the saturable CYP3A-mediated oxidation, in parallel to the previously known CES-mediated hydrolysis. The findings offer an alternative explanation to the well-established intestinal P-gp mediated efflux for the difference in DDI magnitudes of DABE-P-gp inhibitor (CTC and ITZ) following microdose vs therapeutic doses of DABE. The present results also imply that the microdose, unlike the therapeutic dose, of DABE should be used as a dual P-gp and CYP3A, not just P-gp marker substrate when assessing the DDI potential of P-gp and CYP3A inhibitors. Finally, the present study highlights another example of different result interpretations following the microdose vs the therapeutic dose, and suggests the need to establish linearity in pharmacokinetics and characterize associated disposition determinants of a compound over its intended study dose range.

Acknowledgments

We would like to thank Cuyue Tang, Ph.D. and Dan Cui, Ph.D. for their suggestion and critical reviews of this article.

Data Availability Statement

The authors declare that all the data supporting the findings of this study are available within the paper and its Supplemental Data.

Author contributions

Participated in research design: Udomnilobol, Prueksaritanont

Conducted experiments: Udomnilobol

Performed data analysis: Udomnilobol

Wrote or contributed to the writing of the manuscript: Udomnilobol, Jianmongkol,
Prueksaritanont

References

- Blech S, Ebner T, Ludwig-Schwellinger E, Stangier J, and Roth W (2008) The metabolism and disposition of the oral direct thrombin inhibitor, dabigatran, in humans. *Drug Metab Dispos* **36**:386-399.
- Bohnert T, Patel A, Templeton I, Chen Y, Lu C, Lai G, Leung L, Tse S, Einolf HJ, Wang YH, Sinz M, Stearns R, Walsky R, Geng W, Sudsakorn S, Moore D, He L, Wahlstrom J, Keirns J, Narayanan R, Lang D, and Yang X (2016) Evaluation of a new molecular entity as a victim of metabolic drug-drug interactions-an industry perspective. *Drug Metab Dispos* **44**:1399-1423.
- Burt T, Young G, Lee W, Kusuvara H, Langer O, Rowland M, and Sugiyama Y (2020) Phase 0/microdosing approaches: time for mainstream application in drug development? *Nat Rev Drug Discov* **19**:801-818.
- Delavenne X, Ollier E, Basset T, Bertolotti L, Accassat S, Garcin A, Laporte S, Zufferey P, and Mismetti P (2013) A semi-mechanistic absorption model to evaluate drug-drug interaction with dabigatran: application with clarithromycin. *Br J Clin Pharmacol* **76**:107-113.
- EMA (2012) European Medicines Agency. Guideline on the investigation of drug interactions. *Committee for Human Medicinal Products (CHMP)*.
- FDA (2010a) US Food and Drug Administration. Pradaxa: Clinical pharmacology and biopharmaceutics review(s). *Center for Drug Evaluation and Research (CDER)*.
- FDA (2010b) US Food and Drug Administration. Pradaxa: Pharmacology review(s). *Center for Drug Evaluation and Research (CDER)*.
- FDA (2020a) US Food and Drug Administration. Guidance for industry: Clinical drug interaction studies — Cytochrome P450 enzyme- and transporter-mediated drug interactions. *Center for Drug Evaluation and Research (CDER)*.

- FDA (2020b) US Food and Drug Administration. Guidance for industry: In vitro drug interaction studies — Cytochrome P450 enzyme- and transporter-mediated drug interactions. *Center for Drug Evaluation and Research (CDER)*.
- Hartter S, Sennewald R, Nehmiz G, and Reilly P (2013) Oral bioavailability of dabigatran etexilate (Pradaxa®) after co-medication with verapamil in healthy subjects. *Br J Clin Pharmacol* **75**:1053-1062.
- Hatley OJD, Jones CR, Galetin A, and Rostami-Hodjegan A (2017) Quantifying gut wall metabolism: methodology matters. *Biopharm Drug Dispos* **38**:155-160.
- Hodin S, Basset T, Jacqueroux E, Delezay O, Clotagatide A, Perek N, Mismetti P, and Delavenne X (2018) In vitro comparison of the role of p-glycoprotein and breast cancer resistance protein on direct oral anticoagulants disposition. *Eur J Drug Metab Pharmacokinet* **43**:183-191.
- Hu ZY, Parker RB, Herring VL, and Laizure SC (2013) Conventional liquid chromatography/triple quadrupole mass spectrometry based metabolite identification and semi-quantitative estimation approach in the investigation of in vitro dabigatran etexilate metabolism. *Anal Bioanal Chem* **405**:1695-1704.
- Ishiguro N, Kishimoto W, Volz A, Ludwig-Schwellinger E, Ebner T, and Schaefer O (2014) Impact of endogenous esterase activity on in vitro p-glycoprotein profiling of dabigatran etexilate in Caco-2 monolayers. *Drug Metab Dispos* **42**:250-256.
- Ke A, Zamek-Gliszczyński M, Higgins J, and Hall S (2014) Itraconazole and clarithromycin as ketoconazole alternatives for clinical CYP3A inhibition studies. *Clin Pharmacol Ther* **95**:473-476.
- Laizure SC, Parker RB, Herring VL, and Hu ZY (2014) Identification of carboxylesterase-dependent dabigatran etexilate hydrolysis. *Drug Metab Dispos* **42**:201-206.

- Lang J, Vincent L, Chenel M, Ogungbenro K, and Galetin A (2021) Reduced physiologically-based pharmacokinetic model of dabigatran etexilate-dabigatran and its application for prediction of intestinal P-gp-mediated drug-drug interactions. *Eur J Pharm Sci* **165**:105932.
- Obach RS and Reed-Hagen AE (2002) Measurement of Michaelis constants for cytochrome P450-mediated biotransformation reactions using a substrate depletion approach. *Drug Metab Dispos* **30**:831-837.
- Prueksaritanont T, Tatosian DA, Chu X, Railkar R, Evers R, Chavez-Eng C, Lutz R, Zeng W, Yabut J, Chan GH, Cai X, Latham AH, Hehman J, Stypinski D, Brejda J, Zhou C, Thornton B, Bateman KP, Fraser I, and Stoch SA (2017) Validation of a microdose probe drug cocktail for clinical drug interaction assessments for drug transporters and CYP3A. *Clin Pharmacol Ther* **101**:519-530.
- Rattanacheeworn P, Kerr SJ, Kittanamongkolchai W, Townamchai N, Udomkarnjananun S, Praditpornsilpa K, Thanusuwannasak T, Udomnilobol U, Jianmongkol S, Ongpipattanakul B, Prueksaritanont T, Avihingsanon Y, and Chariyavilaskul P (2021) Quantification of CYP3A and drug transporters activity in healthy young, healthy elderly and chronic kidney disease elderly patients by a microdose cocktail approach. *Front Pharmacol* **12**:726669.
- Tatosian DA, Yee KL, Zhang Z, Mostoller K, Paul E, Sutradhar S, Larson P, Chhibber A, Wen J, Wang YJ, Lassman M, Latham AH, Pang J, Crumley T, Gillespie A, Marricco NC, Marengo T, Murphy M, Lasseter KC, Marbury TC, Tweedie D, Chu X, Evers R, and Stoch SA (2021) A microdose cocktail to evaluate drug interactions in patients with renal impairment. *Clin Pharmacol Ther* **109**:403-415.
- van Nuland M, Rosing H, Huitema ADR, and Beijnen JH (2019) Predictive value of microdose pharmacokinetics. *Clin Pharmacokinet* **58**:1221-1236.

- Vermeer LM, Isringhausen CD, Ogilvie BW, and Buckley DB (2016) Evaluation of ketoconazole and its alternative clinical CYP3A4/5 inhibitors as inhibitors of drug transporters: the in vitro effects of ketoconazole, ritonavir, clarithromycin, and itraconazole on 13 clinically-relevant drug transporters. *Drug Metab Dispos* **44**:453-459.
- Yasuda K, Lan LB, Sanglard D, Furuya K, Schuetz JD, and Schuetz EG (2002) Interaction of cytochrome P450 3A inhibitors with P-glycoprotein. *J Pharmacol Exp Ther* **303**:323-332.

Footnotes

This research was supported by the Health System Research Institute [Grant number 60-094], Thailand. All authors declare that they have no competing interests.

Figure legends:

Figure 1: Metabolic conversion from DABE to DAB in human. The bold and dashed arrows indicate the major and minor pathways of DAB formation, respectively.

Figure 2: Metabolic stability of DABE (A), BIBR0951 (B), and BIBR1087 (C) following incubation of 1 μ M in HIM (left panel) and HLM (right panel). The compounds are represented by the symbols as follows: DABE (circle), BIBR0951 (diamond), BIBR1087 (square), and DAB (triangle). Black symbols and solid lines represent the incubations with NADPH, whereas white symbols and dashed lines represent the incubations without NADPH. Data are expressed as % of compounds presented in the incubations, compared to their parents at 0 min (mean \pm SD from $n \geq 3$).

Figure 3: Profiling of BIBR0951 metabolites. The extracted ion chromatograms of BIBR0951 and its metabolites detected in the HIM (A), HLM (B), rhCYP3A4 (C), and rhCYP3A5 (D) incubations with (left panel) or without (right panel) NADPH.

Figure 4: Profiling of DABE metabolites. The extracted ion chromatograms of DABE and its metabolites detected in the HIM (A), HLM (B), rhCYP3A4 (C), and rhCYP3A5 (D) incubations with (left panel) or without (right panel) NADPH.

Figure 5: Effects of KTZ (1 μ M) and BNPP (100 μ M) on the disappearance of DABE in HIM (A), BIBR0951 in HIM (B) and BIBR0951 in HLM (C) in the presence (left panel) or absence (right panel) of NADPH. Data are expressed as % of compounds at 0 min (mean \pm SD from $n = 3$).

Figure 6: Proposed scheme of metabolic conversion from DABE to DAB following oral administration of microdose DABE in human. The bold and dashed arrows indicate the major and minor disposition pathways of microdose DABE, respectively. The plain arrow (non-dashed, non-bold) indicates the potentially minor pathway.

Tables

Table 1: Intrinsic clearance (CL_{int}) of DABE, BIBR0951, and BIBR1087 in HIM and HLM incubations with or without NADPH, and in the presence or absence of inhibitors.

Compounds	Inhibitors	CL_{int} in HIM ($\mu\text{L}/\text{min}/\text{mg HIM}$)		CL_{int} in HLM ($\mu\text{L}/\text{min}/\text{mg HLM}$)	
		With NADPH	Without NADPH	With NADPH	Without NADPH
DABE	-	$1,178 \pm 84$	$723 \pm 97^*$	$4,834 \pm 440$	$4,720 \pm 425$
	KTZ (1 μM)	$550 \pm 209^\#$	$292 \pm 72^\#$	NA	NA
	BNPP (100 μM)	$542 \pm 62^\#$	$50 \pm 44^{*,\#}$	NA	NA
BIBR0951	-	101 ± 1	0^*	580 ± 13	$280 \pm 34^*$
	KTZ (1 μM)	$12 \pm 43^\#$	0^*	$244 \pm 27^\#$	251 ± 20
	BNPP (100 μM)	89 ± 16	0^*	$345 \pm 33^\#$	$48 \pm 54^{*,\#}$
BIBR1087	-	70 ± 1	$42 \pm 5^*$	17 ± 2	14 ± 2

Data are expressed as mean \pm SD from $n \geq 3$. $^*p < 0.05$ comparing to the incubations with NADPH. $^\#p < 0.05$ comparing to the incubations without inhibitors (solvent control). NA, not applicable; 0 (zero), no disappearance observed.

Table 2: Enzyme kinetic parameters following incubation of either DABE or BIBR0951 in HIM, HLM, rhCYP3A4, and rhCYP3A5.

Metabolic reactions	V_{\max} (pmol/min/unit*)	K_m (μ M)	CL_{int} (μ L/min/unit*)
DABE			
HIM (BIBR0951 formation)	2,347 \pm 21	1.2 \pm 0.04	1,921 \pm 77
HIM (BIBR1087 formation)	301 \pm 2	8.4 \pm 0.6	36 \pm 3
HLM (BIBR0951 formation)	125 \pm 5	3.0 \pm 0.1	42 \pm 1
HLM (BIBR1087 formation)	26,977 \pm 312	9.0 \pm 0.3	2,983 \pm 89
rhCYP3A4 (DABE depletion)	60 \pm 9	1.4 \pm 0.2	44 \pm 3
rhCYP3A5 (DABE depletion)	68 \pm 20	1.1 \pm 0.3	59 \pm 7
BIBR0951			
HIM (DAB formation)	ND	ND	ND
HLM (DAB formation)	184,378 \pm 58,053	518 \pm 196	362 \pm 21
rhCYP3A4 (BIBR0951 depletion)	8.3 \pm 1.2	2.8 \pm 0.6	3.0 \pm 0.3
rhCYP3A5 (BIBR0951 depletion)	1.0 \pm 0.2	0.6 \pm 0.1	1.6 \pm 0.3

All incubations with HIM and HLM were performed in the absence of NADPH, while those with rhCYP3A4/5 were performed in the presence of NADPH. Data are expressed as mean \pm SD from n=3. *Units are either mg of microsomal protein, or pmol of recombinant CYP enzyme. ND, no data due to negligible metabolite formation.

Table 3: Intrinsic clearance (CL_{int}) and relative contribution of CYP3A to overall microsomal metabolism at various concentrations of DABE and BIBR0951 in HIM and/or HLM incubations.

Compounds	Microsomes	Concentration (μ M)	CL_{int} (μ L/min/mg protein)		Contribution of CYP3A (%)
			With NADPH	Without NADPH	
DABE	HIM	1	1,178 \pm 84	723 \pm 97*	38 \pm 9
		10	463 \pm 146 [#]	395 \pm 130 [#]	19 \pm 8 [#]
		100	ND	ND	ND
BIBR0951	HIM	1	101 \pm 1	0*	100
		10	21 \pm 3 [#]	0*	100
		100	8 \pm 1 [#]	0*	100
	HLM	1	580 \pm 13	280 \pm 34*	52 \pm 12
		10	281 \pm 4 [#]	239 \pm 19	15 \pm 6 [#]
		100	59 \pm 16 [#]	67 \pm 10 [#]	0 [#]

Data are expressed as mean \pm SD from n=3. The contribution of CYP3A was calculated by $100 \times (CL_{int} \text{ with NADPH} - CL_{int} \text{ without NADPH}) / (CL_{int} \text{ with NADPH})$. * $p < 0.05$ comparing to the incubations with NADPH. [#] $p < 0.05$ comparing to the incubation at 1 μ M. ND, no data due to precipitation of DABE at the concentration $> 30 \mu$ M. 0 (zero), no disappearance observed.

Figure 1

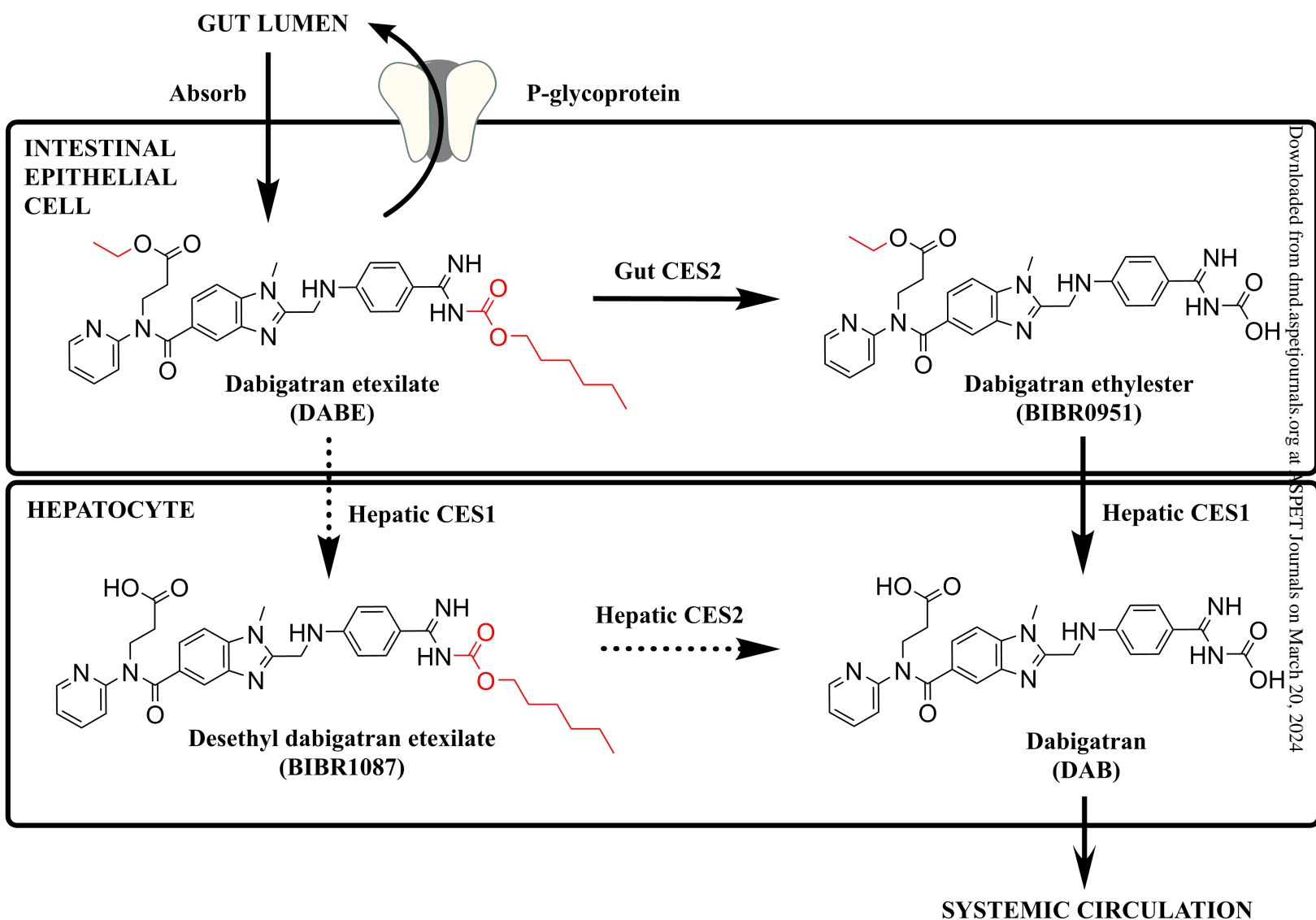


Figure 2

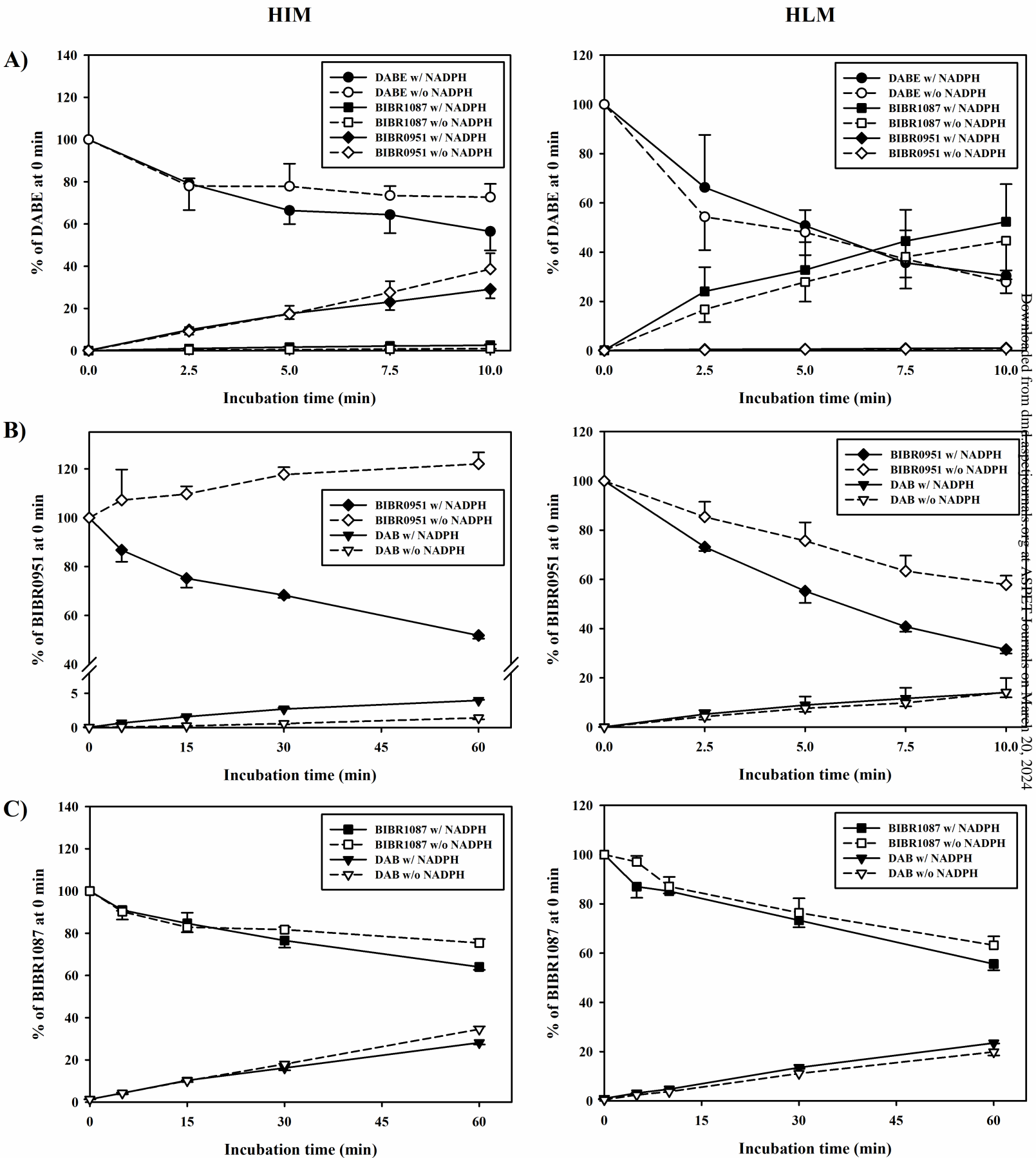


Figure 3

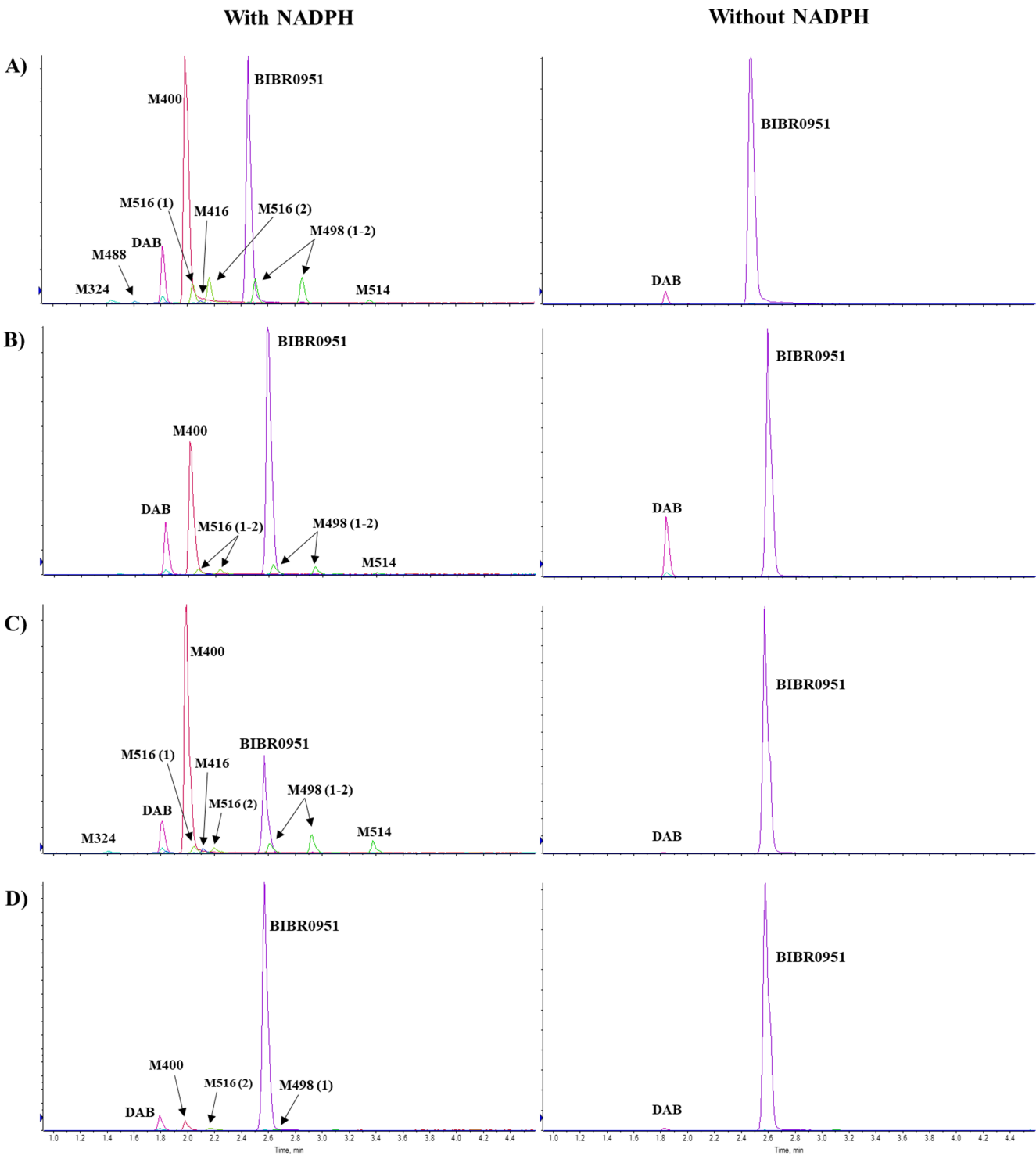


Figure 4

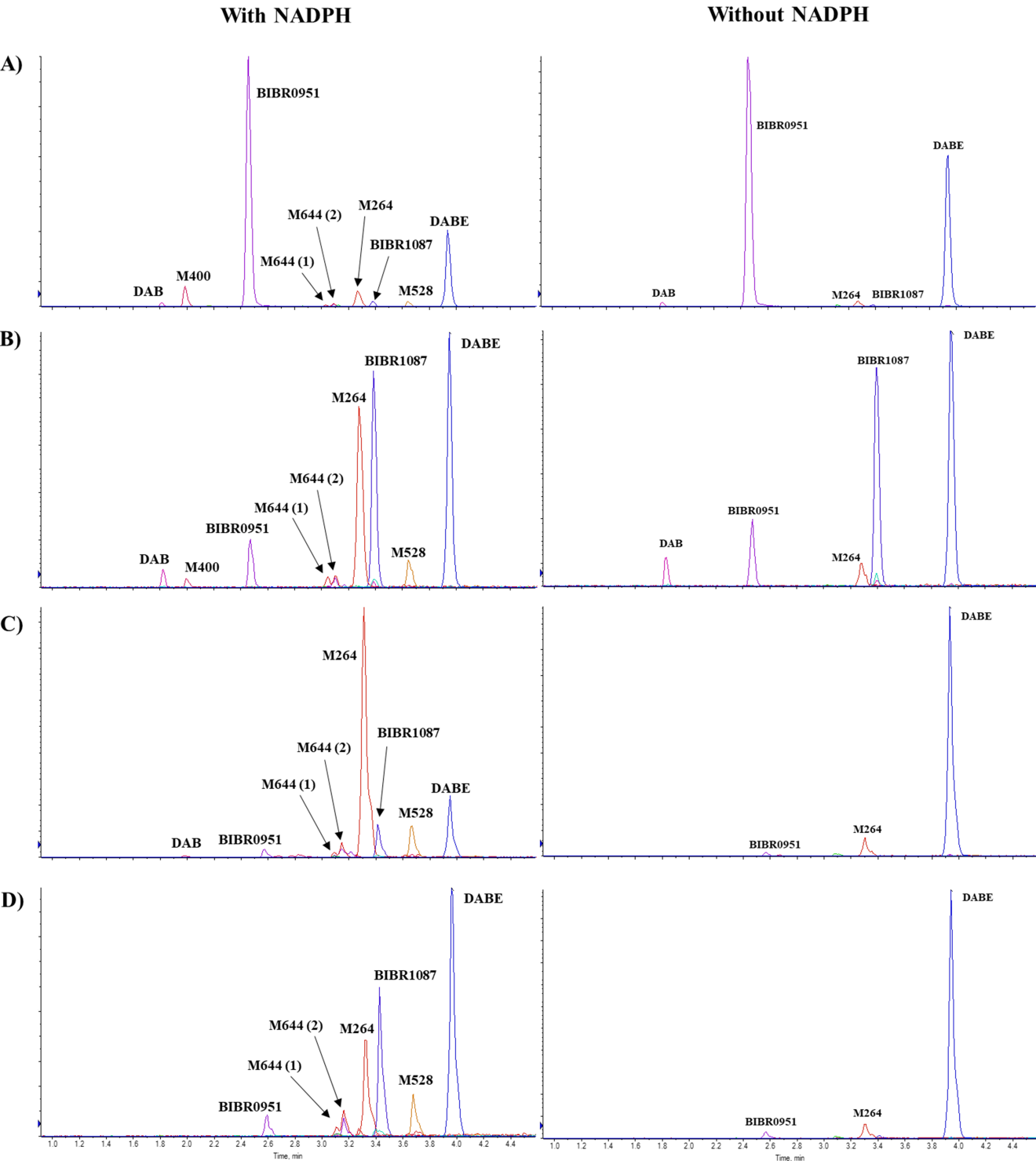


Figure 5

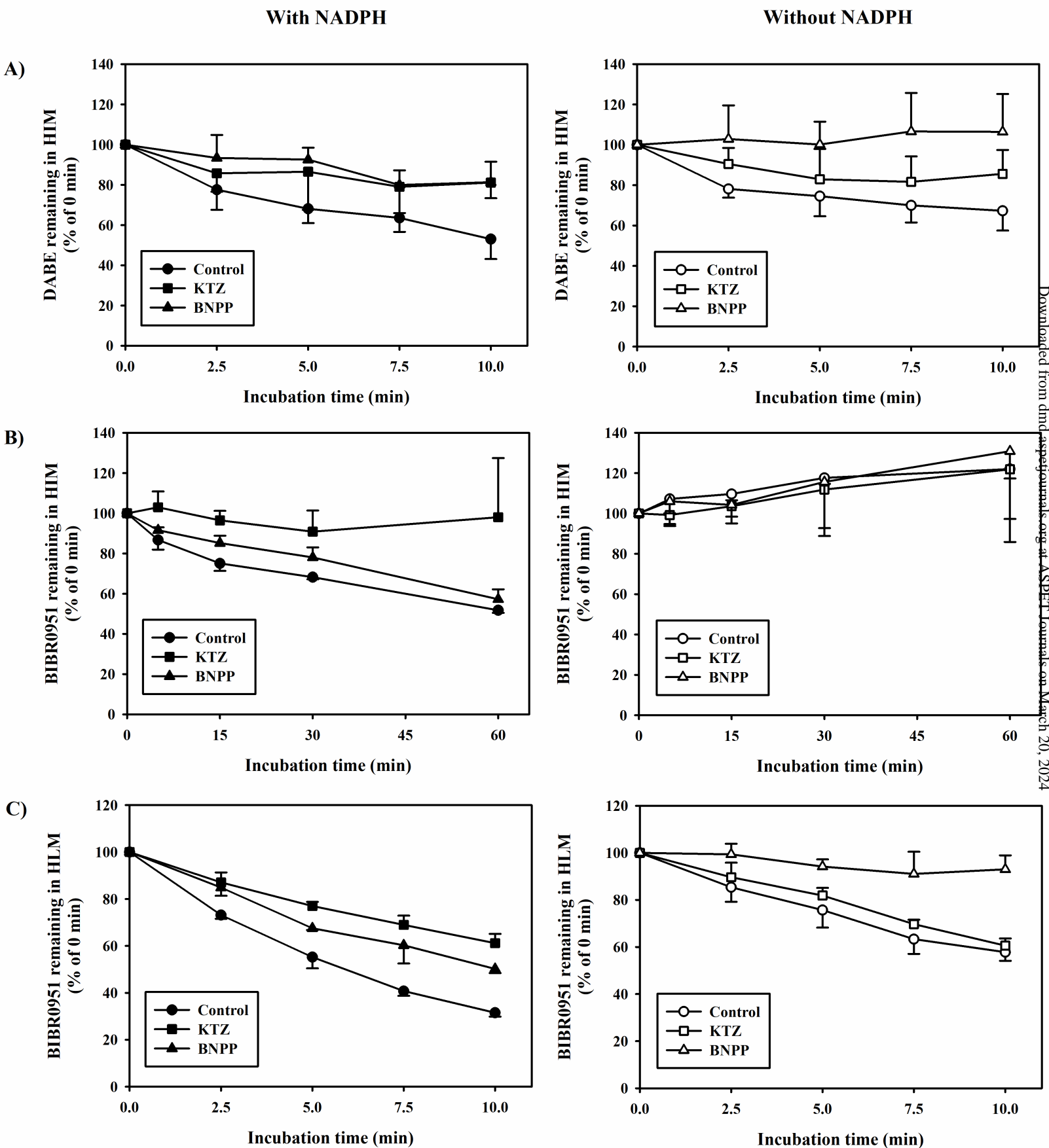
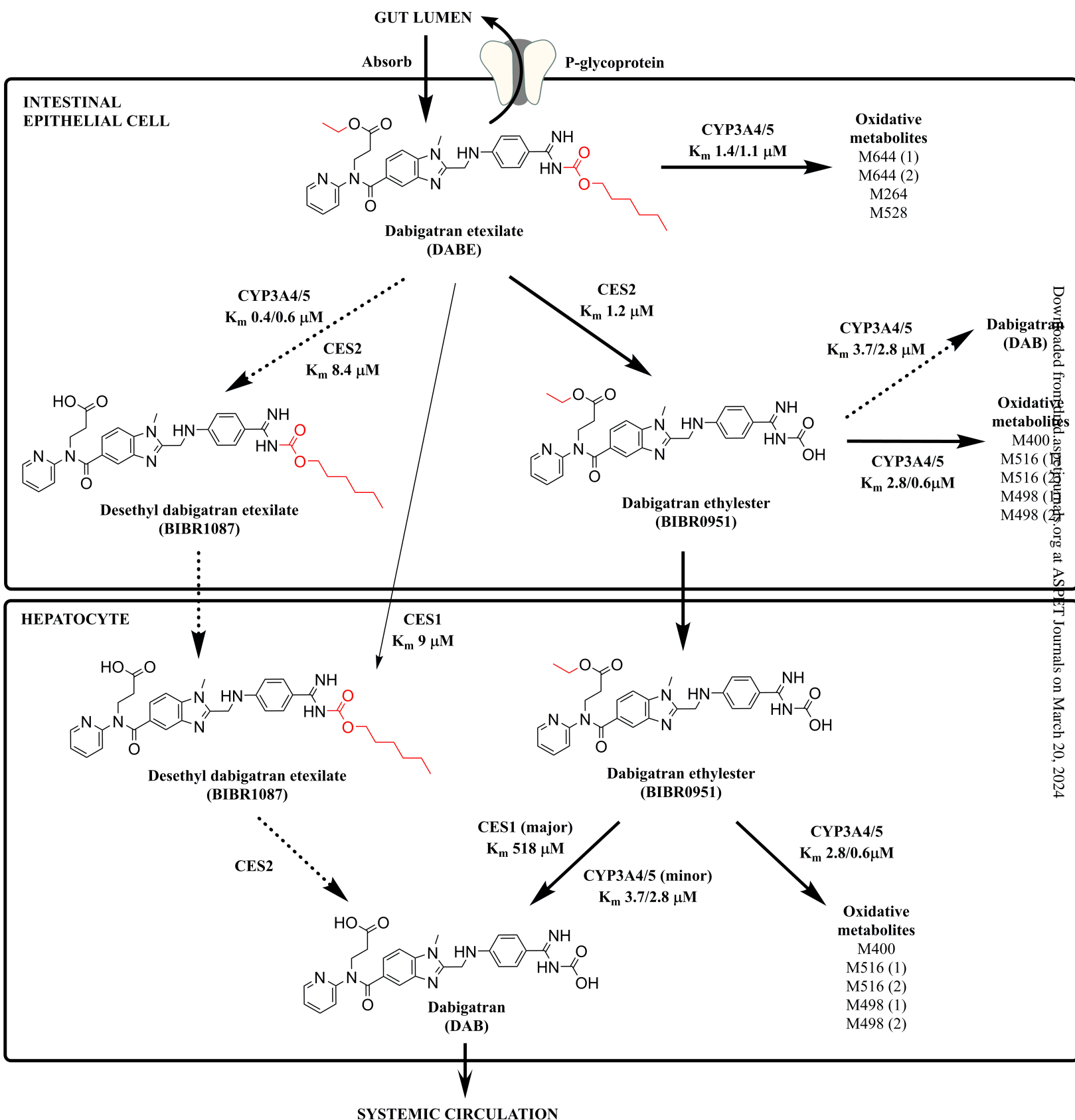


Figure 6



Supplemental data

The Potentially Significant Role of CYP3A-Mediated Oxidative Metabolism of Dabigatran Etexilate and its Intermediate Metabolites in Drug-Drug Interaction Assessments Using Microdose Dabigatran Etexilate

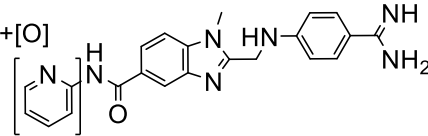
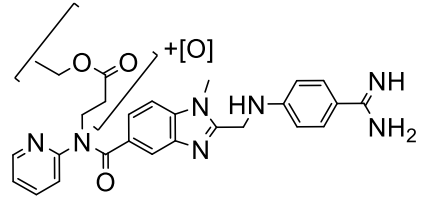
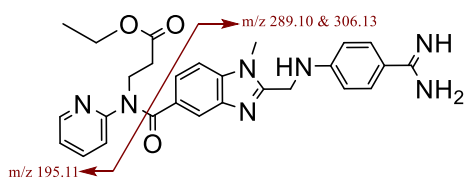
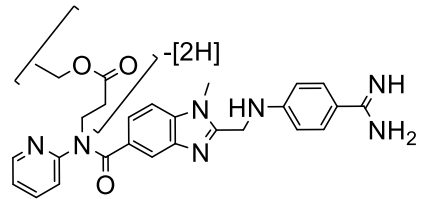
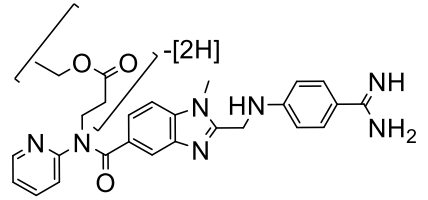
Udomsak Udomnilobol, Suree Jianmongkol, Thomayant Prueksaritanont

Department of Pharmacology and Physiology, Faculty of Pharmaceutical Sciences,
Chulalongkorn University, Bangkok, Thailand (U.U., S.J.).

Chulalongkorn University Drug Discovery and Drug Development Research Center
(Chula4DR), Chulalongkorn University, Bangkok, Thailand (U.U., T.P.).

Supp. Table 1: BIBR0951 and its metabolites detected in the NADPH-fortified incubations.

Species	RT (min)	[M+H] ⁺ m/z (amu)	Structures	Product ion formula [P] ⁺ or [P] ⁺ , m/z (amu)	Detected in*
M324	1.43	[C ₁₇ H ₁₈ N ₅ O ₂] ⁺ 324.1461		[C ₈ H ₇ N ₂] ⁺ , 131.0615; [C ₇ H ₈ N ₂ O] ⁺ , 136.0626; [C ₈ H ₁₀ N ₃] ⁺ , 148.0874; [C ₁₀ H ₉ N ₂ O ₂] ⁺ , 189.0664; [C₁₇H₁₃N₄O]⁺, 289.1079	HIM rhCYP3A4
M488	1.61	[C ₂₅ H ₂₆ N ₇ O ₄] ⁺ 488.2044		[C ₇ H ₈ N ₂ O] ⁺ , 136.0626; [C ₈ H ₁₀ N ₃] ⁺ , 148.0867; [C ₈ H ₉ N ₂ O ₂] ⁺ , 165.0661; [C ₁₀ H ₈ N ₂ O] ⁺ , 172.0651; [C ₁₀ H ₉ N ₂ O ₂] ⁺ , 189.0666; [C₁₇H₁₃N₄O]⁺, 289.1076 ; [C ₁₇ H ₁₆ N ₅ O] ⁺ , 306.1336; [C ₁₇ H ₁₈ N ₅ O ₂] ⁺ , 324.1461	HIM
DAB	1.81	[C ₂₅ H ₂₆ N ₇ O ₃] ⁺ 472.2098		[C ₉ H ₉ N ₂] ⁺ , 145.0765; [C ₈ H ₁₀ N ₃] ⁺ , 148.0871; [C ₁₀ H ₈ N ₂ O] ⁺ , 172.0641; [C ₁₀ H ₉ N ₂ O ₂] ⁺ , 189.0659; [C ₁₅ H ₁₃ N ₄ O] ⁺ , 265.1090; [C ₁₇ H ₁₃ N ₄ O] ⁺ , 289.1086; [C ₁₇ H ₁₆ N ₅ O] ⁺ , 306.1348; [C ₁₇ H ₁₈ N ₅ O ₂] ⁺ , 324.1462; [C ₁₈ H ₁₇ N ₄ O ₃] ⁺ , 337.1303	HLM HIM rhCYP3A4 rhCYP3A5
M400	1.98	[C ₂₂ H ₂₂ N ₇ O] ⁺ 400.1889		[C ₈ H ₇ N ₂] ⁺ , 131.0608; [C ₉ H ₈ N ₂] ⁺ , 144.0686; [C ₈ H ₁₀ N ₃] ⁺ , 148.0872; [C ₁₀ H ₈ N ₂ O] ⁺ , 172.0636; [C ₁₅ H ₁₂ N ₄ O] ⁺ , 264.1011; [C ₁₅ H ₁₃ N ₄ O] ⁺ , 265.1085; [C₁₇H₁₃N₄O]⁺, 289.1086 ; [C ₂₂ H ₁₇ N ₆] ⁺ , 365.1513; [C ₂₂ H ₁₉ N ₆ O] ⁺ , 383.1618	HLM HIM rhCYP3A4 rhCYP3A5
M516 (1)	2.03	[C ₂₇ H ₃₀ N ₇ O ₄] ⁺ 516.2377		[C ₉ H ₉ N ₂] ⁺ , 145.0754; [C ₁₀ H ₈ N ₂ O] ⁺ , 172.0628; [C ₁₆ H ₁₇ N ₅] ⁺ , 279.1482; [C₁₇H₁₃N₄O]⁺, 289.1081 ; [C₁₇H₁₆N₅O]⁺, 306.1342 ; [C ₁₆ H ₁₇ N ₅ O ₂] ⁺ , 311.1372; [C ₁₈ H ₁₇ N ₄ O ₃] ⁺ , 337.1671; [C ₂₅ H ₂₆ N ₇ O ₃] ⁺ , 472.2472	HLM HIM rhCYP3A4

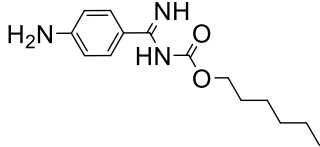
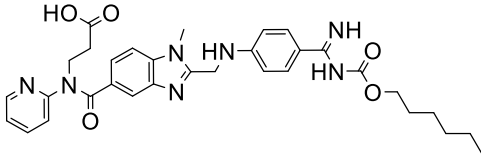
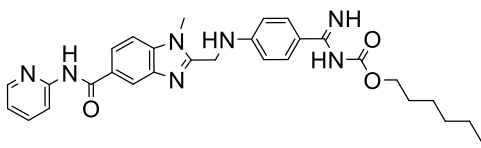
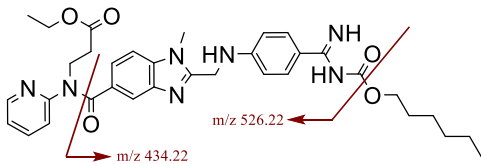
M416	2.10	$[\text{C}_{22}\text{H}_{22}\text{N}_7\text{O}_2]^+$ 416.1834		$[\text{C}_7\text{H}_8\text{N}_2\text{O}]^{*+}$, 136.0621; $[\text{C}_9\text{H}_8\text{N}_2]^{*+}$, 144.0697; $[\text{C}_9\text{H}_9\text{N}_2]^+$, 145.0769; $[\text{C}_{10}\text{H}_8\text{N}_2\text{O}]^{*+}$, 172.0625; $[\text{C}_{17}\text{H}_{13}\text{N}_4\text{O}]^+$, 289.1089 ; $[\text{C}_{17}\text{H}_{16}\text{N}_5\text{O}]^+$, 306.1342	HIM rhCYP3A4
M516 (2)	2.16	$[\text{C}_{27}\text{H}_{30}\text{N}_7\text{O}_4]^+$ 516.2370		$[\text{C}_9\text{H}_9\text{N}_2]^+$, 145.0756; $[\text{C}_8\text{H}_9\text{N}_2\text{O}_2]^+$, 165.0661; $[\text{C}_{10}\text{H}_8\text{N}_2\text{O}]^{*+}$, 172.0638; $[\text{C}_{10}\text{H}_9\text{N}_2\text{O}_2]^+$, 189.0659; $[\text{C}_{10}\text{H}_{13}\text{N}_2\text{O}_2]^+$, 193.0978 ; $[\text{C}_{17}\text{H}_{13}\text{N}_4\text{O}]^+$, 289.1091 ; $[\text{C}_{17}\text{H}_{16}\text{N}_5\text{O}]^+$, 306.1351 ; $[\text{C}_{17}\text{H}_{18}\text{N}_5\text{O}_2]^+$, 324.1456	HLM HIM rhCYP3A4 rhCYP3A5
BIBR0951 (parent)	2.45	$[\text{C}_{27}\text{H}_{30}\text{N}_7\text{O}_3]^+$ 500.2406		$[\text{C}_9\text{H}_8\text{N}_2]^{*+}$, 144.0684; $[\text{C}_9\text{H}_9\text{N}_2]^+$, 145.0764; $[\text{C}_9\text{H}_7\text{N}_2\text{O}]^+$, 159.0556; $[\text{C}_{10}\text{H}_8\text{N}_2\text{O}]^{*+}$, 172.0635; $[\text{C}_{10}\text{H}_{15}\text{N}_2\text{O}_2]^+$, 195.1135 ; $[\text{C}_{15}\text{H}_{12}\text{N}_4\text{O}]^{*+}$, 264.1014; $[\text{C}_{16}\text{H}_{16}\text{N}_5]^+$, 278.1405; $[\text{C}_{17}\text{H}_{13}\text{N}_4\text{O}]^+$, 289.1079 ; $[\text{C}_{17}\text{H}_{16}\text{N}_5\text{O}]^+$, 306.1349 ; $[\text{C}_{22}\text{H}_{17}\text{N}_6]^+$, 365.1614	NA
M498 (1)	2.51	$[\text{C}_{27}\text{H}_{28}\text{N}_7\text{O}_3]^+$ 498.2257		$[\text{C}_9\text{H}_8\text{N}_2]^{*+}$, 144.0672; $[\text{C}_9\text{H}_9\text{N}_2]^+$, 145.0755; $[\text{C}_{10}\text{H}_8\text{N}_2\text{O}]^{*+}$, 172.0639; $[\text{C}_{13}\text{H}_{15}\text{N}_3\text{O}_3]^{*+}$, 261.1147; $[\text{C}_{16}\text{H}_{16}\text{N}_5]^+$, 278.1396; $[\text{C}_{17}\text{H}_{13}\text{N}_4\text{O}]^+$, 289.1089 ; $[\text{C}_{17}\text{H}_{16}\text{N}_5\text{O}]^+$, 306.1351 ; $[\text{C}_{13}\text{H}_{18}\text{N}_4\text{O}_3]^{*+}$, 317.1034	HLM HIM rhCYP3A4 rhCYP3A5
M498 (2)	2.85	$[\text{C}_{27}\text{H}_{28}\text{N}_7\text{O}_3]^+$ 498.2261		$[\text{C}_8\text{H}_7\text{N}_2]^+$, 131.0610; $[\text{C}_9\text{H}_9\text{N}_2]^+$, 145.0762; $[\text{C}_9\text{H}_7\text{N}_2\text{O}]^+$, 159.0562; $[\text{C}_{10}\text{H}_8\text{N}_2\text{O}]^{*+}$, 172.0639; $[\text{C}_9\text{H}_8\text{N}_2\text{O}_2]^{*+}$, 176.0583; $[\text{C}_{17}\text{H}_{13}\text{N}_4\text{O}]^+$, 289.1086 ; $[\text{C}_{17}\text{H}_{16}\text{N}_5\text{O}]^+$, 306.1357 ; $[\text{C}_{13}\text{H}_{18}\text{N}_4\text{O}_3]^{*+}$, 317.1037; $[\text{C}_{25}\text{H}_{22}\text{N}_7\text{O}_2]^+$, 452.1841	HLM HIM rhCYP3A4

M514	3.35	$[\text{C}_{27}\text{H}_{28}\text{N}_7\text{O}_4]^+$ 514.2210		$[\text{C}_6\text{H}_7\text{N}_2\text{O}]^+$, 123.0565; $[\text{C}_7\text{H}_8\text{N}_2\text{O}]^{*+}$, 136.0629; $[\text{C}_9\text{H}_9\text{N}_2]^+$, 145.0765, $[\text{C}_{10}\text{H}_8\text{N}_2\text{O}]^{*+}$, 172.0644; $[\text{C}_{17}\text{H}_{13}\text{N}_4\text{O}]^+$, 289.1106 ; $[\text{C}_{17}\text{H}_{16}\text{N}_5\text{O}]^+$, 306.1360	HLM HIM rhCYP3A4
-------------	------	--	--	---	------------------------

*The metabolites detected in the HLM and rhCYP3A4 incubations at 10 min, or in the HIM and rhCYP3A5 incubations at 60 min. RT, retention time; NA, not applicable.

Supp. Table 2: DABE and its metabolites detected in NADPH-fortified incubations.

Species	RT (min)	[M+H] ⁺ m/z (amu)	Structures	Product ion formula [P] ⁺ or [P] ⁺⁺ , m/z (amu)	Detected in*
DAB	1.82	[C ₂₅ H ₂₆ N ₇ O ₃] ⁺ 472.2094		[C ₇ H ₈ N ₂ O] ⁺⁺ , 136.0619; [C ₉ H ₉ N ₂] ⁺ , 145.0758; [C ₁₀ H ₈ N ₂ O] ⁺⁺ , 172.0638; [C ₁₇ H ₁₃ N ₄ O] ⁺ , 289.1092; [C ₁₇ H ₁₆ N ₅ O] ⁺ , 306.1358; [C ₁₇ H ₁₈ N ₅ O ₂] ⁺ , 324.1452; [C ₁₈ H ₁₇ N ₄ O ₃] ⁺ , 337.1299; [C ₂₂ H ₂₂ N ₇ O] ⁺ , 400.1852	HLM HIM rhCYP3A4
M400	2.00	[C ₂₂ H ₂₂ N ₇ O] ⁺ 400.1891		[C ₈ H ₇ N ₂] ⁺ , 131.0607; [C ₇ H ₈ N ₂ O] ⁺⁺ , 136.0622; [C ₈ H ₁₀ N ₃] ⁺ , 148.0873; [C ₁₀ H ₈ N ₂ O] ⁺⁺ , 172.0637; [C ₁₅ H ₁₂ N ₄ O] ⁺⁺ , 264.1008; [C ₁₅ H ₁₃ N ₄ O] ⁺ , 265.1091; [C ₁₇ H ₁₃ N ₄ O] ⁺ , 289.1087; [C ₂₂ H ₁₇ N ₆] ⁺ , 365.1511; [C ₂₂ H ₁₉ N ₆ O] ⁺ , 383.1621	HLM HIM
BIBR0951	2.47	[C ₂₇ H ₃₀ N ₇ O ₃] ⁺ 500.2411		[C ₉ H ₉ N ₂] ⁺ , 145.0764; [C ₉ H ₇ N ₂ O] ⁺ , 159.0563; [C ₁₀ H ₈ N ₂ O] ⁺⁺ , 172.0637; [C ₁₃ H ₁₅ N ₃ O ₃] ⁺ , 261.1129; [C ₁₅ H ₁₂ N ₄ O] ⁺⁺ , 264.0977; [C ₁₇ H ₁₃ N ₄ O] ⁺ , 289.1090; [C ₁₇ H ₁₆ N ₅ O] ⁺ , 306.1354; [C ₂₂ H ₁₇ N ₆] ⁺ , 365.1636	HLM HIM rhCYP3A4 rhCYP3A5
M644 (1)	3.05	[C ₃₄ H ₄₂ N ₇ O ₆] ⁺ 644.3201		[C ₁₀ H ₈ N ₂ O] ⁺⁺ , 172.0617; [C ₁₇ H ₁₃ N ₄ O] ⁺ , 289.1084; [C ₁₇ H ₁₆ N ₅ O] ⁺ , 306.1375; [C ₁₈ H ₁₄ N ₅ O ₂] ⁺ , 332.1149; [C ₂₇ H ₃₀ N ₇ O ₃] ⁺ , 500.2356; [C ₂₈ H ₂₈ N ₇ O ₄] ⁺ , 526.2182	HLM HIM rhCYP3A4 rhCYP3A5
M644 (2)	3.11	[C ₃₄ H ₄₂ N ₇ O ₆] ⁺ 644.3207		[C ₁₇ H ₁₃ N ₄ O] ⁺ , 289.1079; [C ₁₅ H ₁₉ N ₃ O ₃] ⁺⁺ , 289.1087; [C ₁₇ H ₁₆ N ₅ O] ⁺ , 306.1327; [C ₁₈ H ₁₄ N ₅ O ₂] ⁺ , 332.1152; [C ₂₇ H ₂₈ N ₆ O ₄] ⁺⁺ , 500.2188; [C ₂₇ H ₃₀ N ₇ O ₃] ⁺ , 500.2414; [C ₂₈ H ₂₈ N ₇ O ₄] ⁺ , 526.2192	HLM HIM rhCYP3A4 rhCYP3A5

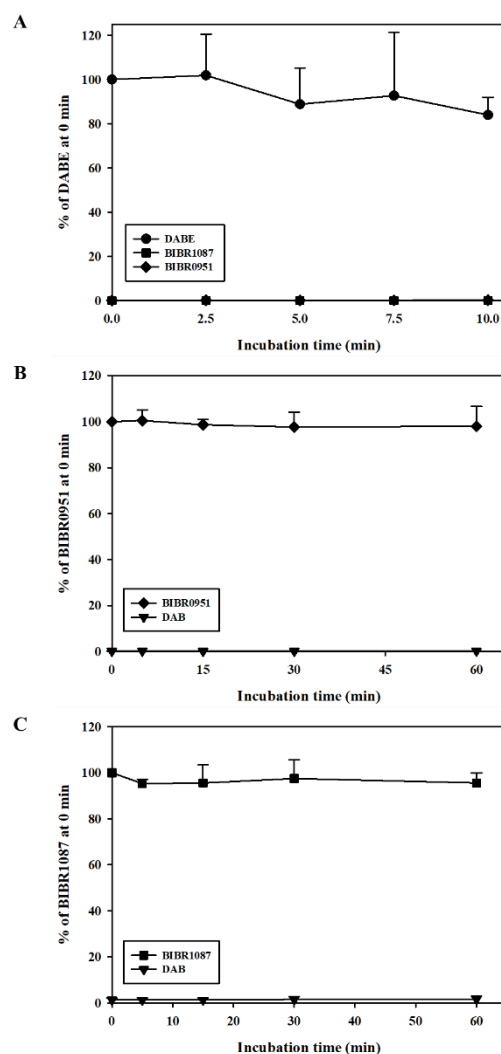
M264	3.28	$[\text{C}_{14}\text{H}_{22}\text{N}_3\text{O}_2]^+$ 264.1707		$[\text{C}_6\text{H}_6\text{N}]^+$, 92.0501; $[\text{C}_7\text{H}_7\text{N}_2]^+$, 119.0608; $[\text{C}_7\text{H}_{10}\text{N}_3]^+$, 136.0872; $[\text{C}_8\text{H}_8\text{N}_3\text{O}]^+$, 162.0673; $[\text{C}_8\text{H}_{10}\text{N}_3\text{O}_2]^+$, 180.0775	HLM HIM rhCYP3A4 rhCYP3A5
BIBR1087	3.39	$[\text{C}_{32}\text{H}_{38}\text{N}_7\text{O}_5]^+$ 600.2928		$[\text{C}_8\text{H}_9\text{N}_2\text{O}]^+$, 149.0715; $[\text{C}_{17}\text{H}_{13}\text{N}_4\text{O}]^+$, 289.1089; $[\text{C}_{17}\text{H}_{16}\text{N}_5\text{O}]^+$, 306.1354; $[\text{C}_{18}\text{H}_{14}\text{N}_5\text{O}_2]^+$, 332.1150; $[\text{C}_{18}\text{H}_{16}\text{N}_5\text{O}_3]^+$, 350.1250; $[\text{C}_{24}\text{H}_{28}\text{N}_5\text{O}_3]^+$, 434.2193; $[\text{C}_{25}\text{H}_{24}\text{N}_7\text{O}_2]^+$, 454.1993	HLM HIM rhCYP3A4 rhCYP3A5
M528	3.64	$[\text{C}_{29}\text{H}_{34}\text{N}_7\text{O}_3]^+$ 528.2727		$[\text{C}_8\text{H}_{10}\text{N}_3]^+$, 148.0871; $[\text{C}_{15}\text{H}_{13}\text{N}_4\text{O}]^+$, 265.1103; $[\text{C}_{17}\text{H}_{13}\text{N}_4\text{O}]^+$, 289.1096 ; $[\text{C}_{17}\text{H}_{16}\text{N}_5\text{O}]^+$, 306.1361; $[\text{C}_{22}\text{H}_{17}\text{N}_6]^+$, 365.1508; $[\text{C}_{22}\text{H}_{19}\text{N}_6\text{O}]^+$, 383.1623; $[\text{C}_{22}\text{H}_{22}\text{N}_7\text{O}]^+$, 400.1887; $[\text{C}_{23}\text{H}_{20}\text{N}_7\text{O}_2]^+$, 426.1675	HLM HIM rhCYP3A4 rhCYP3A5
DABE (parent)	3.95	$[\text{C}_{34}\text{H}_{42}\text{N}_7\text{O}_5]^+$ 628.3240		$[\text{C}_{10}\text{H}_8\text{N}_2\text{O}]^{++}$, 172.0638; $[\text{C}_{10}\text{H}_9\text{N}_2\text{O}_2]^+$, 189.0667; $[\text{C}_{17}\text{H}_{13}\text{N}_4\text{O}]^+$, 289.1091 ; $[\text{C}_{17}\text{H}_{16}\text{N}_5\text{O}]^+$, 306.1359; $[\text{C}_{18}\text{H}_{14}\text{N}_5\text{O}_2]^+$, 332.1149; $[\text{C}_{22}\text{H}_{17}\text{N}_6]^+$, 365.1613; $[\text{C}_{24}\text{H}_{28}\text{N}_5\text{O}_3]^+$, 434.2194 ; $[\text{C}_{28}\text{H}_{28}\text{N}_7\text{O}_4]^+$, 526.2194	NA

*The metabolites detected in the HLM, HIM, rhCYP3A4, and rhCYP3A5 incubations at 10 min. RT, retention time; NA, not applicable.

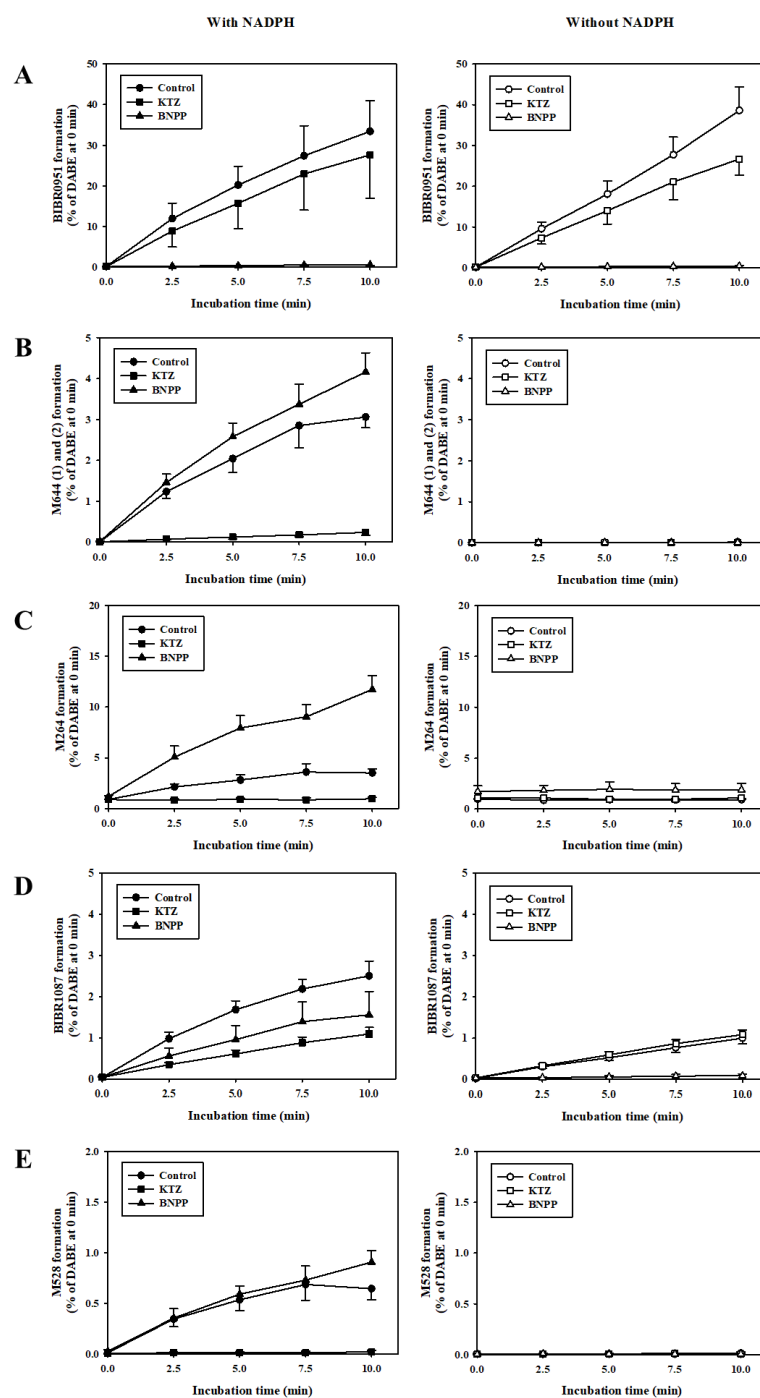
Supp. Table 3: Formation kinetic of primary metabolites following incubation of either DABE or BIBR0951 in NADPH-fortified rhCYP3A4 and rhCYP3A5.

Metabolic reactions	rhCYP3A4			rhCYP3A5		
	V _{max} (pmol/min/pmol)	K _m (μM)	CL _{int} (μL/min/pmol)	V _{max} (pmol/min/pmol)	K _m (μM)	CL _{int} (μL/min/pmol)
DABE						
BIBR0951 formation	ND	ND	ND	ND	ND	ND
M644 (1) and (2) formation	NA	0.6 ± 0.1	NA	NA	0.6 ± 0.04	NA
M264 formation	NA	0.3 ± 0.1	NA	NA	0.3 ± 0.1	NA
BIBR1087 formation	2.7 ± 0.1	0.4 ± 0.04	7.2 ± 0.5	1.4 ± 0.1	0.6 ± 0.1	2.4 ± 0.5
M528 formation	NA	1.4 ± 0.3	NA	NA	2.4 ± 0.2	NA
BIBR0951						
DAB formation	2.6 ± 0.2	3.7 ± 0.5	0.7 ± 0.1	0.9 ± 0.03	2.8 ± 0.3	0.3 ± 0.03
M400 formation	NA	2.9 ± 0.1	NA	NA	1.2 ± 0.1	NA
M516 (1) formation	NA	3.7 ± 0.3	NA	NA	NA	NA
M516 (2) formation	NA	2.8 ± 0.3	NA	NA	1.6 ± 0.4	NA
M498 (1) formation	NA	4.6 ± 0.3	NA	NA	1.1 ± 0.1	NA
M498 (2) formation	NA	3.1 ± 0.3	NA	NA	NA	NA

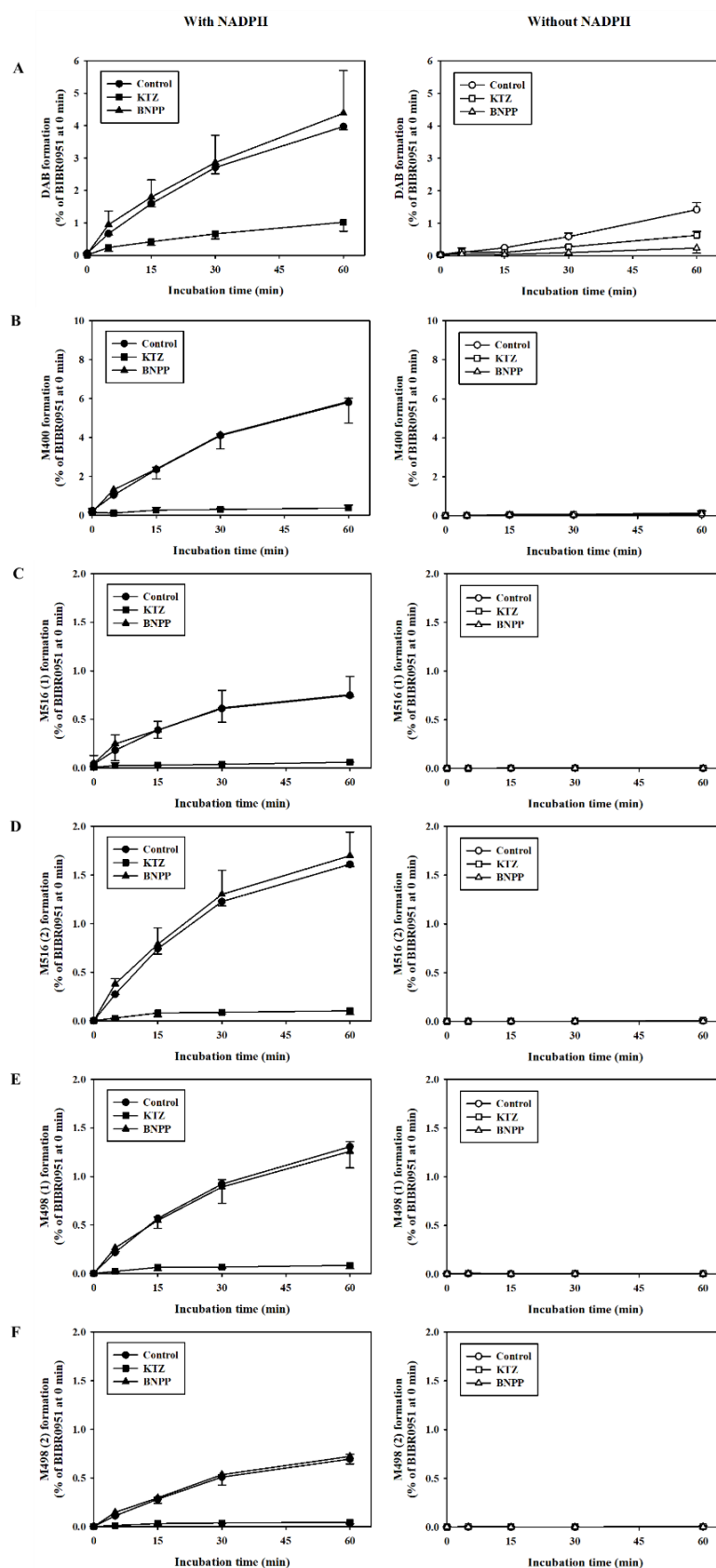
Data are expressed as mean ± SD from n=3. NA, not applicable due to lack of analytical standards. ND, no data due to negligible metabolite formation.



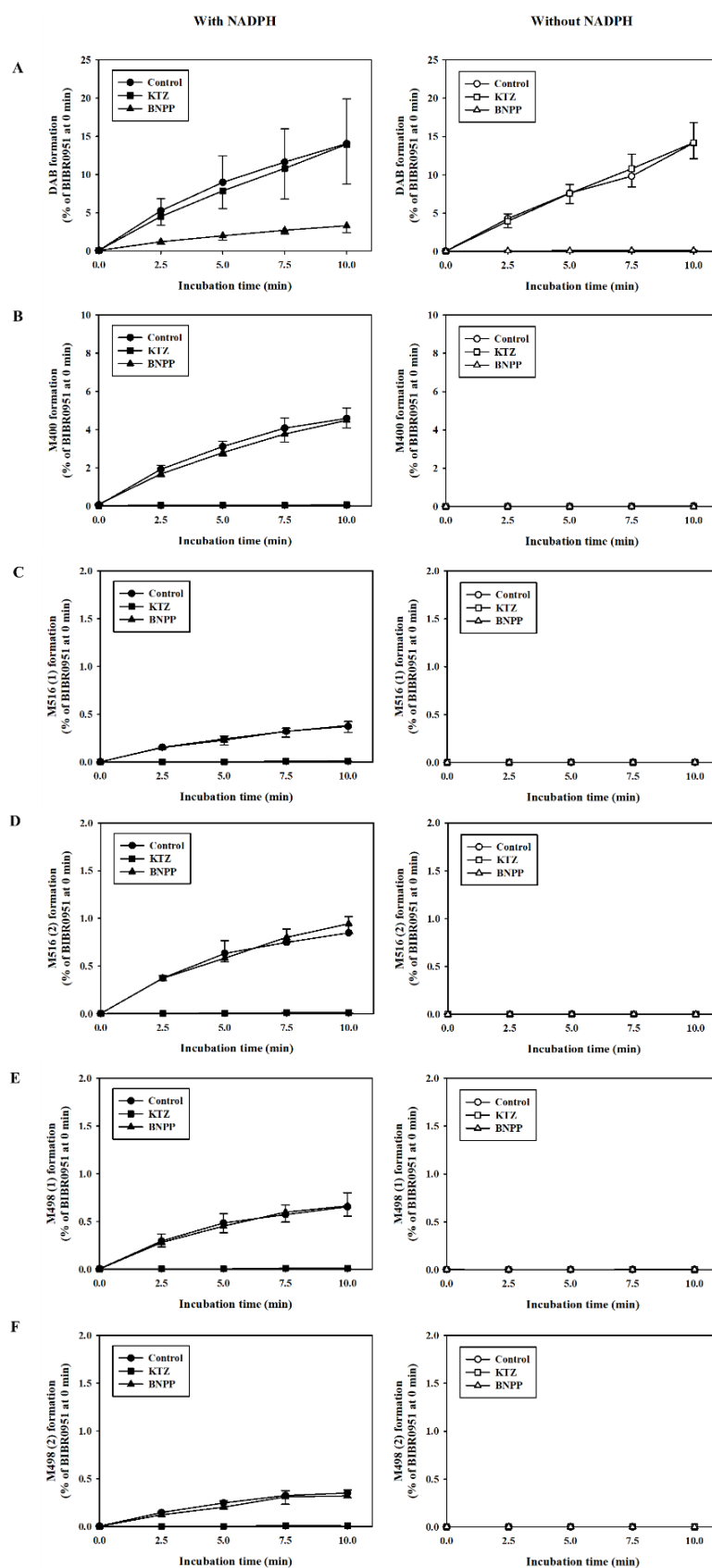
Supp. Figure 1: Stability of DABE (A), BIBR0951 (B), and BIBR1087 (C) in the phosphate buffer fortified with NADPH (no microsomal protein). Data are expressed as mean \pm SD from n=3.



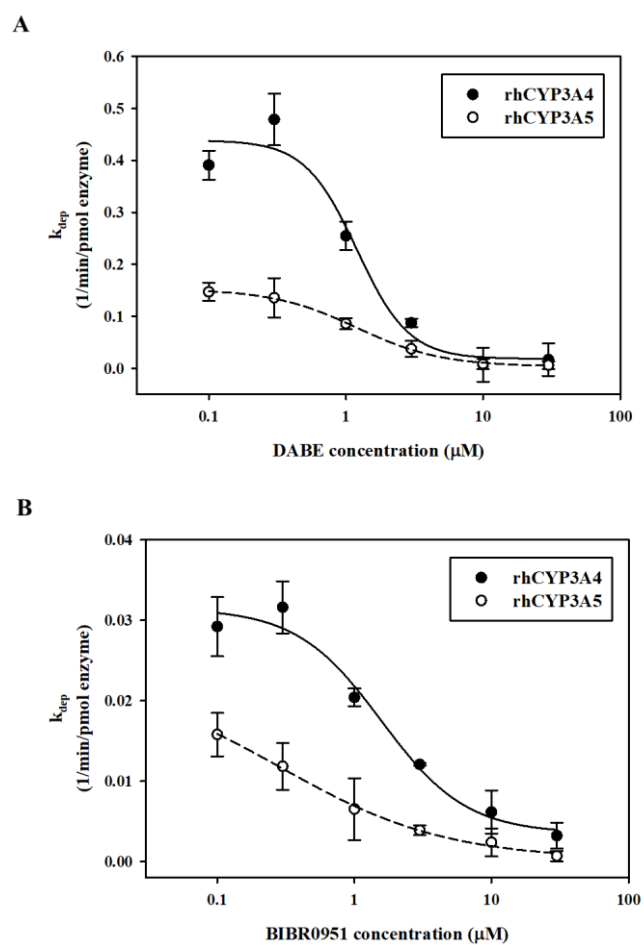
Supp. Figure 2: Effects of KTZ (1 μ M) and BNPP (100 μ M) on the formation of BIBR0951 (A), M644 (1) and (2) (B), M264 (C), BIBR1087 (D), and M528 (E) following incubation of 1 μ M DABE in HIM with (left panel) or without (right panel) NADPH. Data are expressed as mean \pm SD from n=3. The formation of M644 (1) and (2) was combined due to incomplete separation of chromatographic peaks.



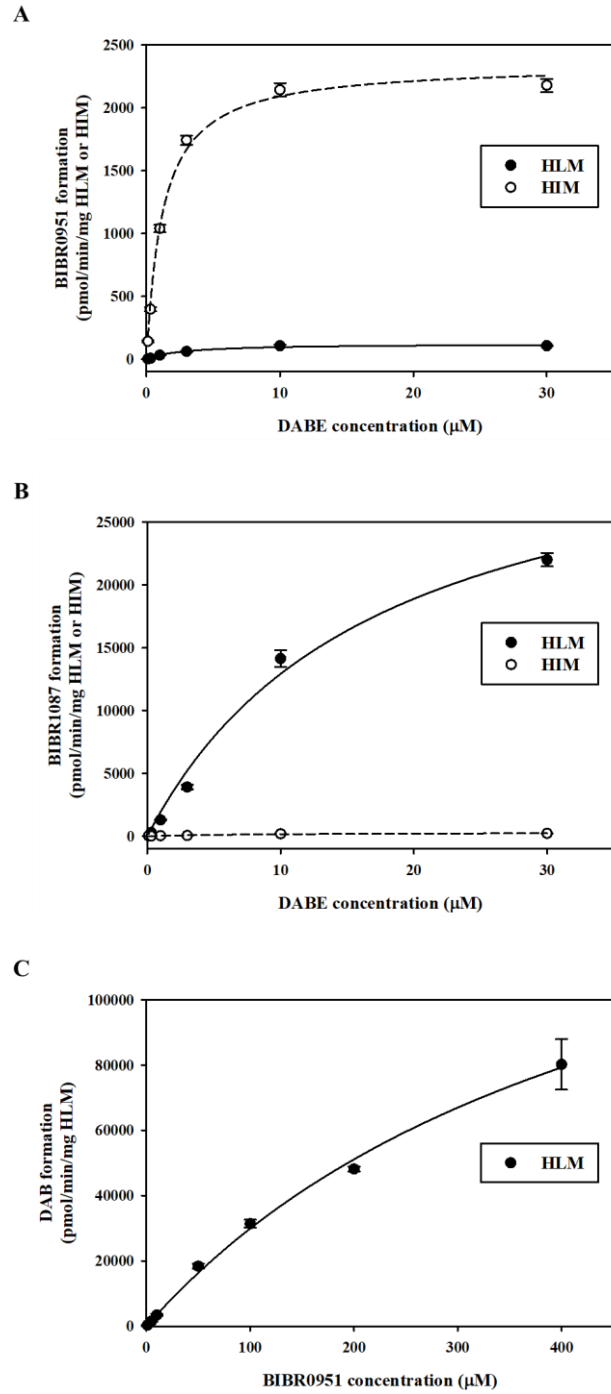
Supp. Figure 3: Effects of KTZ (1 μ M) and BNPP (100 μ M) on the formation of DAB (A), M400 (B), M516 (1) (C), M516 (2) (D), M498 (1) (E), and M498 (2) (F) following incubation of 1 μ M BIBR0951 in HIM with (left panel) or without (right panel) NADPH. Data are expressed as mean \pm SD from n=3.



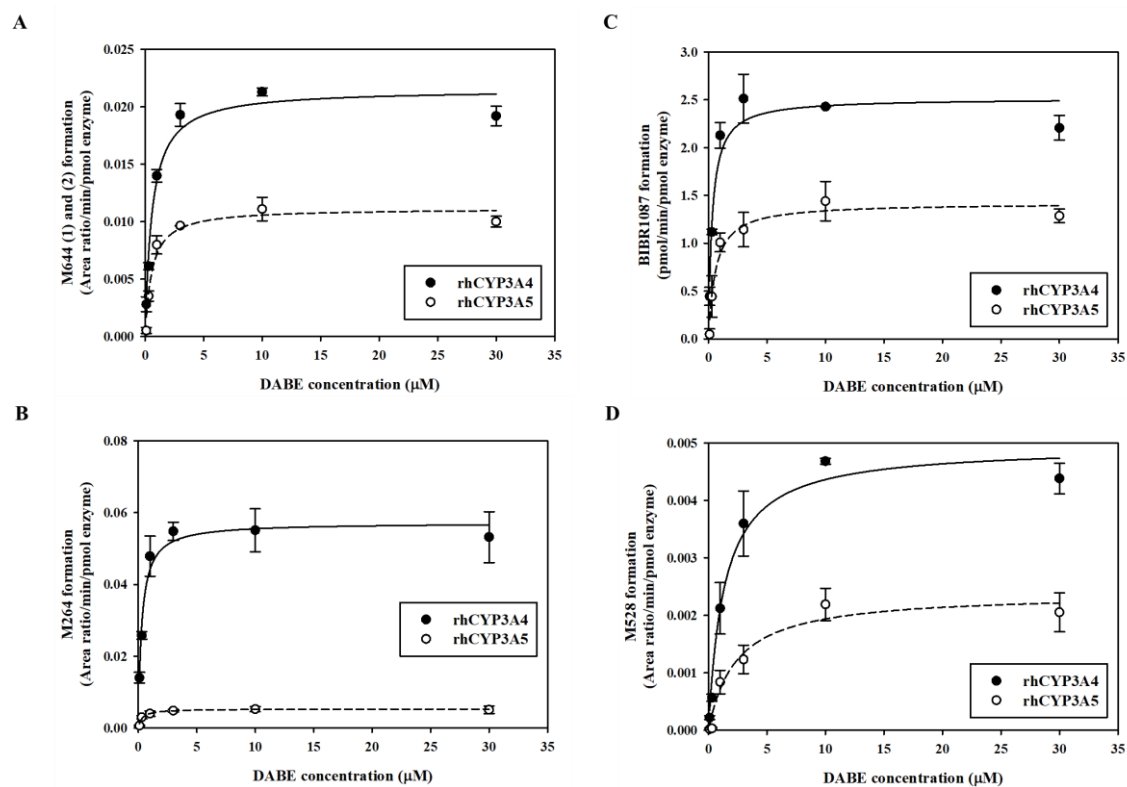
Supp. Figure 4: Effects of KTZ (1 μ M) and BNPP (100 μ M) on the formation of DAB (A), M400 (B), M516 (1) (C), M516 (2) (D), M498 (1) (E), and M498 (2) (F) following incubation of 1 μ M BIBR0951 in HLM with (left panel) or without (right panel) NADPH. Data are expressed as mean \pm SD from n=3.



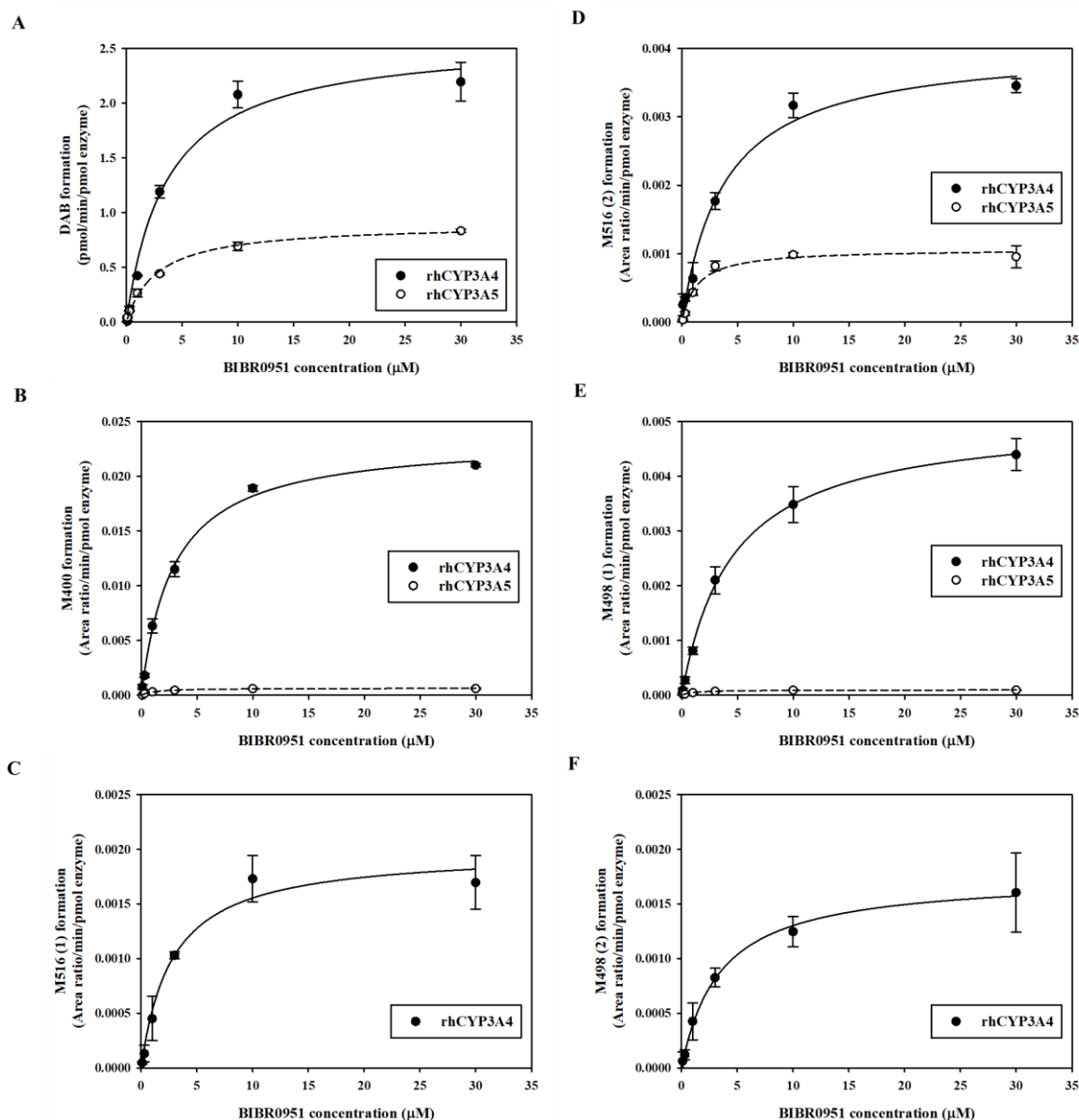
Supp. Figure 5: Plots of *in vitro* depletion rate constants (k_{dep}) of DABE (A) and BIBR0951 (B) versus concentrations in the NADPH-fortified rhCYP3A4 and rhCYP3A5 systems. Data are expressed as mean \pm SD from $n=3$.



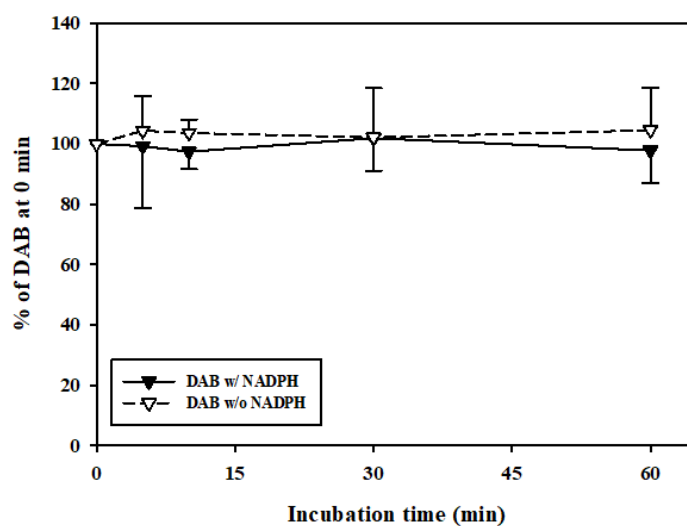
Supp. Figure 6: Michaelis-Menten kinetics of CES-mediated hydrolysis of DABE (A and B) and BIBR0951 (C) in HLM and HIM. Data are expressed as mean \pm SD from n=3. The DAB formation was negligible in the HIM incubation with BIBR0951.



Supp. Figure 7: The formation of M644 (1) and (2) (A), M264 (B), BIBR1087 (C), and M528 (D) following incubation of DABE in NADPH-fortified rhCYP3A4 and rhCYP3A5 systems. Data are expressed as mean \pm SD from $n=3$. The formation of M644 (1) and (2) was combined due to incomplete separation of chromatographic peaks.



Supp. Figure 8: The formation of DAB (A), M400 (B), M516 (1) (C), M516 (2) (D), M498 (1) (E), and M498 (2) (F) following incubation of BIBR0951 in NADPH-fortified rhCYP3A4 and rhCYP3A5 systems. Data are expressed as mean \pm SD from n=3. M516 (1) and M498 (2) were not formed in the rhCYP3A5 system.



Supp. Figure 9: Metabolic stability of DAB (1 μ M) in HLM (0.5 mg/mL). Black symbols and solid lines represent the incubations with NADPH, whereas white symbols and dashed lines represent the incubations without NADPH. Data are expressed as % of DAB compared to 0 min (mean \pm SD from n = 3).